Bioactive Materials 28 (2023) 206–226

Contents lists available at ScienceDirect

Bioactive Materials

journal homepage: www.keaipublishing.com/en/journals/bioactive-materials

Dual human iPSC-derived cardiac lineage cell-seeding extracellular matrix patches promote regeneration and long-term repair of infarcted hearts

Yun Jiang [a,b], Ling-Ling Zhang [b], Fan Zhang [c], Wei Bi [b], Peng Zhang [a,b], Xiu-Jian Yu [b], Sen-Le Rao [b], Shi-Hui Wang [b], Qiang Li [a,b], Chen Ding [c], Yin Jin [b], Zhong-Min Liu [a], Huang-Tian Yang [a,b,d,*]

[a] Translational Medical Center for Stem Cell Therapy & Institute for Heart Failure and Regenerative Medicine, Shanghai East Hospital, School of Medicine, Tongji University, Shanghai, 200092, China
[b] CAS Key Laboratory of Tissue Microenvironment and Tumor, Shanghai Institute of Nutrition and Health, University of Chinese Academy of Sciences (CAS), CAS, Shanghai, 200031, PR China
[c] State Key Laboratory of Genetic Engineering and Collaborative Innovation Center for Genetics and Development, School of Life Sciences, Institute of Biomedical Sciences, Human Phenome Institute, Zhongshan Hospital, Fudan University, Shanghai, 200433, China
[d] Institute for Stem Cell and Regeneration, CAS, Beijing, 100101, PR China

ARTICLE INFO

Keywords:
Induced human pluripotent stem cells
Cardiac lineage cells
Extracellular matrix patch
Cardiomyocyte regeneration
Infarcted heart repair

ABSTRACT

Human pluripotent stem cell-derived cardiovascular progenitor cells (hCVPCs) and cardiomyocytes (hCMs) possess therapeutic potential for infarcted hearts; however, their efficacy needs to be enhanced. Here we tested the hypotheses that the combination of decellularized porcine small intestinal submucosal extracellular matrix (SIS-ECM) with hCVPCs, hCMs, or dual of them (Mix, 1:1) could provide better therapeutic effects than the SIS alone, and dual hCVPCs with hCMs would exert synergic effects in cardiac repair. The data showed that the SIS patch well supported the growth of hCVPCs and hCMs. Epicardially implanted SIS-hCVPC, SIS-hCM, or SIS-Mix patches at 7-day post-myocardial infarction significantly ameliorated functional worsening, ventricular dilation and scar formation at 28- and 90-day post-implantation in C57/B6 mice, whereas the SIS only mildly improved function at 90-day post-implantation. Moreover, the SIS and SIS-cell patches improved vascularization and suppressed MI-induced cardiomyocyte hypertrophy and expression of *Col1* and *Col3*, but only the SIS-hCM and the SIS-Mix patches increased the ratio of collagen III/I fibers in the infarcted hearts. Further, the SIS-cell patches stimulated cardiomyocyte proliferation via paracrine action. Notably, the SIS-Mix had better improvements in cardiac function and structure, engraftments, and cardiomyocyte proliferation. Proteomic analysis showed distinct biological functions of exclusive proteins secreted from hCVPCs and hCMs, and more exclusive proteins secreted from co-cultivated hCVPCs and hCMs than mono-cells involving in various functional processes essential for infarct repair. These findings are the first to demonstrate the efficacy and mechanisms of mono- and dual-hCVPC- and hCM-seeding SIS-ECM for repair of infarcted hearts based on the side-by-side comparison.

1. Introduction

Heart failure (HF) following myocardial infarction (MI) remains a leading cause of morbidity and mortality worldwide [1]. Current treatments improve the symptoms and survival but cannot compensate for the MI-caused irreversible loss of contractile myocardial tissue due to extensive cardiomyocyte loss and massive vascular disruption [2,3]. Cell therapy by implantation of stem/progenitor cells and their derived cardiovascular cells offers new opportunities for repair of infarcted hearts [3–8]. However, more studies are needed to determine suitable cell types, mechanisms underlying, and optimal approaches for enhancing the therapeutic efficacy and safety of cell therapy for infarcted hearts.

Among various implantable cells, cardiovascular lineage cells derived from human pluripotent stem cells (hPSCs), including human embryonic stem cells (hESCs) and human induced pluripotent stem cells

Peer review under responsibility of KeAi Communications Co., Ltd.
* Corresponding author. Stem Cells and Cardiac Repair, Shanghai Institute of Nutrition and Health, CAS, Shanghai, 200031, PR China.
E-mail address: htyang@sinh.ac.cn (H.-T. Yang).

https://doi.org/10.1016/j.bioactmat.2023.05.015
Received 6 December 2022; Received in revised form 21 May 2023; Accepted 22 May 2023

(hiPSCs), are promising sources for promoting repair of infarcted hearts, with the aims of stimulating endogenous repair mechanisms and providing healthy cardiovascular cells [4,5,7,9,10]. Accumulating evidence demonstrates improvements of cardiac function and reduction of fibrosis formation after implantation of hPSC-derived cardiovascular progenitor cells (hCVPCs) or cardiomyocytes (hCMs) at acute and subacute stages of MI in rodent infarcted hearts [11–13]. The efficacy of these cells for improving cardiac function, revascularization and/or remuscularization of infarcted hearts are further confirmed in MI models of non-human primates (NHP) [4,5,10] and swine [14,15]. The safety of first clinical trials using of hCVPCs [16] and hCM patches [17] in patients with severe ischemic cardiomyopathy have been reported. However, the low engraftment of hCVPCs and incidence of ventricular arrhythmias following intramyocardial injection of hCMs derived from hPSCs or NHP iPSCs were observed in NHP and swine models of MI [4,5,10,13,15]. Whether these cells share comparable therapeutic effects for infarcted hearts and implantation of dual hCVPCs and hCMs would exert synergistic beneficial effects for infarcted hearts need to be investigated.

Because MI causes loss of not only cardiomyocytes but also myocardial tissue and the infarct scar expands with the thinner infarcted wall, the cardiac patches by use of hCMs or cell combinations with tissue-derived extracellular matrix (ECM) have been explored. The ECM provides a critical microenvironment that supports cell survival and function as well as promotes adaptive reparative processes of damaged cardiovascular tissues [18–20]. Implantation of hCM and vessel cell-fibrin patches does not adversely affect the electrical stability of infarcted swine hearts [14]. Decellularized ECM scaffold from intact porcine small intestinal submucosa (SIS)-ECM has superior biocompatibility as well as naturally structural, mechanical, and biochemical properties [18,19,21,22]. It releases various growth factors after implanted to MI hearts of rodents [19,23] and large animals [24,25] to stimulate paracrine responses, vascularization, and reparative inflammatory response and has been utilized in clinic for paediatric cardiovascular surgery and aortic valve replacement [26,27]. The SIS-ECM material, containing various types of ECM components, supports physical attachment and active growth for cells, such as human bone marrow-derived mesenchymal stem cells (BMMSCs) [21], mouse ESC-derived Isl1$^+$ cardiac progenitor cells (mCPCs) [28], and neonate cardiac progenitor cells [29]. However, it is unknown whether the SIS-ECM can support the survival of hCVPCs and hCMs and whether these cell-seeding SIS patches can promote the repair of infarcted hearts better than the SIS-ECM alone.

To address above questions, in the present study, we did side-by-side comparison of epicardial implantation of the SIS patches alone and the SIS-seeded hiPSC-derived hCVPC-, hCM-, and hCVPC + hCM (Mix) patches at 7 days post-MI in a mouse model of MI to determine (i) the biocompatibility of the SIS to hCVPCs and hCMs; (ii) therapeutic efficacy of epicardial implantation of hCVPC-, hCM-, and Mix-seeding SIS-patches as well as SIS alone for infarcted hearts; and (iii) mechanisms underlying the promotion of cardiac repair mediated by these treatments. The results from this study confirmed the feasibility of seeding hPSC-derived mono- and dual-cardiac lineage cells on the SIS patches, demonstrate similar and unique characteristics of therapeutic effects, and revealed paracrine mechanisms of the mono- and dual-hCVPC + hCM-seeding SIS patches for infarct repair. These findings would provide the new knowledge and approaches for promotion of infarct healing.

2. Methods

2.1. Construction of a green fluorescent protein (GFP$^+$) hiPSC reporter line

The hiPSCs, generated as we previously reported [30], were used to generate GFP$^+$ hiPSCs with the CRISPR/Cas9 system to insert a GFP-T2A-luciferase sequence into the genomic safe harbor AAVS1 site as previously reported [31]. Briefly, the sequence "CACCGGGTCTTCGAGAAGACCTGTTT" was inserted into *Bbs*I restriction site of pX459 (#48139) to construct pX459-AAVS1. The sequence between *Sal*I and *Mlu*I of pAAVS1-CAG-hrGFP (#52344) was replaced with GFP-T2A-luciferase sequence to construct a pAAVS1-CAG-GFP-T2A-Luc vector. The hiPSCs were nucleofected with the pX459-AAVS1 and pAAVS1-CAG-GFP-T2A-Luc plasmids. Then the hiPSCs were selected with puromycin at 48 h post-nucleofection, and selected 5000 cells were re-plated in a 10 cm dish supplemented with Rho-associated protein kinase inhibitor Y-27632 (Sigma-Aldrich, Carlsbad, USA) to maintain cell viability. About 2 weeks later, the single cell-derived clones were large enough to be picked and then amplified. The hiPSCs expressing GFP were confirmed by puromycin selection, immunocytochemical staining and flow cytometry analysis.

2.2. hiPSC culture and cardiac lineage cell differentiation

The hiPSCs were routinely maintained in mTeSR medium (Stem Cell Technologies) on Matrigel-coated plates. The induction of hCVPCs from hiPSCs was followed the protocol reported previously [4,12,32,33]. Briefly, undifferentiated hiPSCs were dissociated with Accutase (Stem Cell Technologies), and then plated onto Matrigel-coated culture dishes at a density of 5×10^4 cells/cm^2 in hCVPC-induction medium (DMEM/F12, 1 × B27 supplement without vitamin A, 1% L-Glutamine, 1% penicillin/streptomycin, 400 μM 1-thioglycerol, 50 μg/mL ascorbic acid, 25 ng/mL bone morphogenetic protein 4, and 3 μM CHIR99021). The hCVPCs were harvested after 3 days of differentiation and characterized by the expression of sialyl-glycolipid stage-specific embryonic antigen 1 (SSEA1), mesoderm posterior bHLH transcription factor 1 (MESP1), GATA binding protein 4 (GATA4), ISL LIM homeobox 1 (ISL1), and NK2 homeobox 5 (NKX2-5).

The hCM induction from hiPSCs was followed the protocol reported previously [34] with the differentiation medium (Complete RPMI) consisted of RPMI-1640 media (Life Technologies, 11875–085) supplemented with B27® minus insulin (Life Technologies, A1895601) (RPMI + B27–I). On the first day (D0) of differentiation, CHIR 99021 (LC Laboratories, C-6556) at 6 μM was added and maintained for two days. On D2, the media was aspirated and replaced with RPMI + B27–I. On D3, the media was aspirated and replaced with 5 μM of IWR-1 in RPMI + B27–I. On D5, the media was replaced with RPMI + B27–I and RPMI plus B27 supplemented with insulin (RPMI + B27) on D7. The hCMs were generally began spontaneously beating on D7 and maintained in RPMI + B27 with a medium change every other day. Then the hCMs were characterized by the expression of cardiac troponin T (cTnT), cardiac troponin I (cTnI), and α-actinin. hCMs were purified with glucose-depleted culture medium containing abundant lactate as described previously [35].

2.3. Alkaline phosphatase (ALP) staining

The ALP activity was determined with an ALP substrate kit III (Vector Laboratories, Burlingame, CA, USA) as we previously described [36,37]. Briefly, the hiPSC clones were fixed in 4% paraformaldehyde and incubated with the fresh vector blue substrate solution for 30–45 min according to the manufacture's instruction. The colonies were imaged with a microscope after washing with the PBS.

2.4. Immunocytochemical staining

The immunocytochemical staining were performed according to the protocol described previously [4,38]. Briefly, cells seeded on slides or SIS patches were fixed with 4% paraformaldehyde (4% PFA) and permeabilized in 0.4% Triton X-100 (Sigma). After blocking with 10% normal goat serum (Vector Laboratories), the cells were then incubated with primary antibodies against octamer-binding transcription factor 4 (OCT4, Abcam, ab19857, 1:100), nanog homeobox (NANOG, Abcam,

ab21624, 1:100), SSEA4 (Millipore, MAB4304,1:300), MESP1 (Abcam, ab77013, 1:100), ISL1 (Abcam, ab178400, 1:200), and NKX2-5 (Abcam, ab91196, 1:200), cTnT (Abcam, ab8295, 1:400), cTnI (Abcam, ab47003, 1:400), α-actinin (Abcam, ab9465, 1:400), or GATA4 (Stem Cell, SC-25310, 1:100) in 4 °C overnight and detected by DyLight 488- or 549-conjugated secondary antibodies. Nuclei were stained with Hoechst33258 (Sigma). Zeiss fluorescence microscope was used for slide observation and image capture.

2.5. Flow cytometry analysis and fluorescence-activated cell sorting (FACS)

The hiPSCs, hCVPCs and hCMs analyzed by flow cytometry as previously described [32,33,37] and incubated with antibodies: PE-conjugated SSEA4 (eBioscience, 12-8843-42, 1:100), PE-conjugated SSEA1 (eBioscience, 12-8813-42, 1:50), or un-conjugated cTnT (Abcam, ab8295, 1:200) and ki67 (Abcam, ab16667, 1:200) with PE-conjugated secondary antibody (eBioscience, 12-4010-87, 1:200) or isotype-matched negative controls. Cells were then analyzed by FACS (FACS tar Plus Flow Cytometer, Becton-Dickinson, San Jose, CA, USA).

Cell sorting was performed using a FACS sorter (Beckman Moflo Astrios) based on the SSEA1 detection as we reported previously [37]. Briefly, The Mix cells were dissociated 0.05% Trypsin-EDTA (Thermo Fisher Scientific) for 5 min at 37 °C and washed once with the wash buffer (1% FBS in Dulbecco's phosphate-buffered saline, DPBS, Invitrogen, 14190144) after collected. The cells were then incubated with the primary antibody (PE-conjugated SSEA1, eBioscience, 12-8813-42, 1:50) for 1 h at 4 °C after blocking. Then the suspensions were filtered with a 40 μm cell strainer and sorted using Beckman Moflo flow cytometer. The $SSEA1^+$ cells (Mix-hCVPCs) and $SSEA1^-$ cells (Mix-hCMs) were collected and used for further analysis.

2.6. Preparation of cell-seeding SIS patches

The hCVPCs (D3), hCMs (D20-D23), and cell mixtures (Mix, hCVPCs: hCMs, 1 : 1) were seeded on the matrigel pre-coated SIS patches in 5 mm width and 9 mm length (Shanghai Baiyiyuan Bioengineering Company) with the cell density of $3 \times 10^5/cm^2$ to make cell-seeding SIS patches (about 2×10^5 cells total in the SIS patch), named SIS-hCVPC, SIS-hCM, and SIS-Mix patches, respectively. The SIS and cell-seeding SIS patches were cultured at 37 °C with 5% CO_2 for 36–42 h before implantation.

2.7. Cells viability analysis

To determine the biocompatibility of SIS with hCVPCs, hCMs, and Mix, the cell viability was measured with Cell Counting Kit-8 (CCK-8, Dojindo Laboratories, Cko4) as we previously described [39]. Briefly, the culture medium was replaced with 200 μL fresh medium containing 20 μL CCK-8 following the instructions after cultivation of the SIS or cell-seeding SIS patches in 24-well plate overnight. Then, the cells were incubated for 4 h at 37 °C with 5% CO_2 followed by the absorbance read at 450 nm as a reference wavelength to indicate the cell viability state. Each CCK8 assay repeated three times.

2.8. MI model and study designs

All surgical procedures were performed in accordance with the Guidelines for Care and Use of Laboratory Animals published by the US National Institutes of Health (NIH Publication, 8th Edition, 2011) and were approved by the Institutional Animal Care and Use Committee of Shanghai Institutes of Nutrition and Health. Male C57BL/6J mice (8–10 weeks, purchased from the Shanghai Slac Laboratory Animal Co. Ltd., China) were maintained in a specific-pathogen-free environment.

The MI surgery was performed as previously described [12,40]. Briefly, male mice aged 11–12 weeks were anesthetized with intraperitoneal injection of 50 mg/kg sodium pentobarbital, and ventilated with a volume regulated respirator (SAR830, Cwe Incorporated). The body temperature was maintained at 37 °C and the MI model was induced by permanent ligation of the left anterior descending (LAD) coronary artery with a 7-0 silk sutures. One-week post-MI, the C57BL/6J mice with LV ejection fraction (LVEF) between 30% and 45% were randomly divided into following groups. For comparing the cardiac function between the SIS-hCVPC patches and intramyocardial injection of hCVPCs: (i) MI control (MI Ctrl) group with the second thoracotomy operation; (ii) intramyocardial injection of hCVPCs in a total of 20 μL of PBS suspension into two sites of the border zone (10 μL per site) (hCVPC-Inj); and (iii) epicardial implantation of SIS-hCVPC patches (SIS-hCVPCs). For comparing the therapeutic effects of the SIS and SIS-cell patches for infarct repair: (i) MI control (MI Ctrl), (ii) SIS alone (SIS), (iii) SIS seeded with hCVPCs (SIS-hCVPCs), (iv) SIS seeded with hCMs (SIS-hCMs), and (v) SIS seeded with both hCVPCs and hCMs (SIS-Mix). The SIS with or without cells were epicardially implanted onto the mouse infarcted hearts (Video S1) at 7 days post-MI and examined at 28 days or 90 days post-implantation. All cell implantation groups were with the equal number of cells (2×10^5). All animals were intraperitoneally administrated with cyclosporine A (CSA, 10 μg/g/day) at 1 day before implantation and 8 days afterwards as previously reported [41].

Supplementary video related to this article can be found at https://doi.org/10.1016/j.bioactmat.2023.05.015

2.9. Echocardiography

Transthoracic echocardiography (Vevo 2100, Visual Sonics) with a 25-MHz imaging transducer was performed on anesthetized animals as previously described [12,38,40]. Echocardiographic evaluation was performed 7 days post-MI (as a baseline before implantation) and 7, 28, 60, 90 days post-implantation (D7, D28, D60, D90) by measurements of LVEF, LV fractional shortening (LVFS), LV end-systolic dimension (LVESD), and LV end-diastolic dimension (LVEDD). Hearts were imaged in 2D long-axis view at the level of the greatest LV diameter which used to position the M-mode image.

2.10. Electrocardiograms monitoring

Animals were placed in a chamber and fixed on the table connected to a small rodent ventilator for subsequent electrocardiogram monitoring. Then the electrocardiograms were continuously using a PowerLab system for 30 min at one day before MI, after MI and implantation (7 days post-MI). The raw electrocardiogram traces were viewed in the LabChart software to count the number of arrhythmic events.

2.11. Preparation of heart tissue samples

The hearts were quickly removed from anesthetized mice and washed with 5 mL cold cardiac arresting buffer (10% KCl), 1 × PBS to collect samples as we previously reported [12]. For heart sections, the ventricular tissues were cut and fixed with 4% PFA solution for 1 h before embedded in OCT (SAKURA). Between the point of ligation and the apex of the heart, transversal sections (6 μm thickness each) were prepared at 400 μm intervals. Two sections in each heart from the same layer were used for histological staining and the same parts were photographed in the different groups. For RNA extraction, the ventricular tissues were homogenized using Trizol following the manufacturer's instructions and cDNA was generated by reverse transcription of total RNA (1 μg) using ReverTra Ace reverse transcriptase (Toyobo) for further analysis.

2.12. Quantitative reverse transcription polymerase chain reaction (RT-qPCR)

The total RNA was extracted from cells according to the protocol as we described before [36]. Briefly, total RNA was prepared using

RNAprep Pure Micro Kit (TIANGEN BIOTECH) following the manufacturer's instructions. cDNA was generated by reverse transcription of total RNA (1 μg) using ReverTra Ace reverse transcriptase (Toyobo) and qPCR was performed and analyzed by kinetic real-time PCR using the ABI PRISM 7900 system (Applied Biosystems) with SYBR Green Real-time PCR Master Mix plus (Roche). The transcript of reduced glyceraldehyde-phosphate dehydrogenase (GAPDH) was used for internal normalization. The primers are listed in Table S1.

2.13. Quantification of cell retention

To detect the cell retention in short term after implantation, the level of hGAPDH in the total RNA extracted from the LV tissue was calculated by RT-qPCR according to the protocol described previously [12]. The transcript of mGAPDH was used for internal normalization. n = 5 for each time point in each group. The RT-qPCR primers were listed in Table S1.

The cell retention at 1 day, 28 days, and 90 days post-implantation were identified for GFP^+ cells by fluorescent immunohistochemistry (IHC) staining as previously described [42]. The cell retention was expressed as the total number of GFP^+ cells in each heart divides the number of implanted cells (2×10^5). For quantitation, two sections each heart and the same layer among four hearts each group were analyzed.

2.14. Masson's trichrome, picrosirius red (PSR), and hematoxylin and eosin (H&E) staining

The Masson's trichrome staining analysis was performed as we previously described [12]. Briefly, the frozen heart sections were fixed and stained with the Masson's trichrome kit (G1340-100, Solarbio) and the morphometric parameters were blindly analyzed on three sections from the point of ligation to the apex of each heart. The scar size was calculated as total scar area divided by the LV area with image-processing software (Image Pro Plus5.0) and 6–7 hearts for each group were assessed.

For evaluation of collagen content, heart sections were stained with picrosirius red according to the manufacturers' instructions (BP-DL030, Nanjing SenBeiJia) and the polarized images were obtained using Analyzer module DIC ACR P&C for polarized light microscopy (Zeiss) as described previously [43], in which the orange or red birefringence represent for thicker cross-linked fibers and green for thinner fibers. Then, the respective proportions of different hues were assessed using Image J software as following hue definitions: red or orange 2-38 and 230–256, yellow 39–51, green 52–128. The number of pixels was calculated as a percentage of the total number of collagen pixels. For quantitation, 12–14 views from 6 to 7 hearts each were assessed to quantitate polarized collagen at 28 days post-implantation.

To examine whether presence of red blood cells within arterioles, an indicative of blood perfusion as previously reported [44], in the SIS patches, the heart sections were stained with hematoxylin-eosin (Sigma-Aldrich) and separately stained with an *anti*-α-SMA antibody according to the manufacturer's instruction.

2.15. Fluorescent IHC staining

Fluorescent IHC staining was performed as we previously reported [12,38–40]. The fresh frozen sections were fixed with 4% PFA, permeabilized in 0.4% Triton X-100 (Sigma), and incubated with the following antibodies overnight at 4 °C: *anti*-GFP (Abcam, ab13970, 1:400), cTnT, α-smooth muscle actin positive (α-SMA, Abcam, ab5694, 1:400), platelet endothelial cell adhesion molecule-1(CD31, Abcam, ab28364, 1:200), ki67 (Abcam, ab16667, 1:200), phosphorylated histone 3 (PH3, CST, #9701, 1:100), Aurora B kinase (Aurora B, Abcam, ab2254, 1:100), and FITC-conjugated Wheat Germ Agglutinin (WGA, Sigma, L4895, 1:100) antibodies. Antibodies were detected by fluorescent-conjugated secondary antibodies. Nuclei were stained with Hoechst33258 (Sigma). Histological images were blindly measured using a Zeiss inverted microscope and processed using ZEN software. The density of vessels was evaluated by counting the number of vascular structures that were positive for α-SMA expression per square millimeter or CD31 area per HPF as we previously reported [38,39]. Proliferation was evaluated by counting the number of cells that expressed both ki67 and cTnT per HPF as previously described [14]. For quantitation, 5 hearts (2 sections each heart) for each group were assessed to quantitate vessels and proliferative cardiomyocytes, and total at least 500 cardiomyocytes from 10 sections were count to quantitate cell size.

2.16. Preparation of conditioned media (CdM)

The CdM from cultivated SIS or cell-seeding SIS patches were prepared as we previously reported [12,40]. The SIS and SIS-hCVPCs, SIS-hCMs, and SIS-Mix were cultured for 24 h. Then the media were changed to 1.5 mL serum-free DMEM after thoroughly washed with 1 × PBS 3 times. After incubation for 48 h, the culture media were collected as the CdM after the cells were removed by centrifuge in 1000 g for 10 min.

2.17. Tube formation and migration assays

The tube formation was evaluated with human umbilical vein endothelial cells (HUVECs, Shanghai Zhongqiao XinZhou Biotechnology) as we previously reported [40]. Briefly, in a 48-well, 200 μL of matrigel was coated at 37 °C for 1 h to solidify, then HUVECs were seeded onto matrigel-coated 48-well plates (4×10^4 cells/well) and cultivated with fresh DMEM medium or various CdMs in 5% CO_2 at 37 °C for 24 h. Independent experiments were performed for 5 times and 3 random images from each well were blindly analyzed using ImageJ Angiogenesis Analyzer (National Institutes of Health, Bethesda, Maryland) to quantify the tube length formed.

The migration of HUVECs was examined by using scratch wound-healing assay as we previously described [40] with a slight modification. Briefly, HUVCEs were seeded at a density of 4×10^4 cells/well on 1% gelatin (Sigma, G1890) coated 12-well plates and cultured in DMEM/F12 (Invitrogen, 11330057) supplemented with 1% FBS (Gibco, 10099) at 37 °C and 5% CO_2 until 100% confluence. A gap in the confluent monolayer was induced by scratching with a 20 μL pipette tip and washed three times with PBS. Then the PBS or CdM with equal volume was added into the plates and the scratched areas were captured by using a microscope (Nikon-ECLIPSE Ti, Nikon Corporation, Tokyo, Japan) before and after treatments for 12 h and analyzed (ImageJ). The migration ability was calculated as ((0 h area - 12 h area)/0 h area) × 100%. Independent experiments were performed for 5 times.

2.18. Cell proliferation analysis

The proliferation assessment was performed as previously described [14]. The hCMs (D20-D25) were seeded onto chamber slides in 24-well plates (1×10^5 cells/well) (ThermoFisher Scientific) that had been pre-coated with matrigel and cultured at 37 °C in DMEM or CdM for 2 days. Then the 4% PFA-fixed cells were used for immunocytochemical staining of cTnT and proliferation marker ki67. Independent experiments were performed for 3 times and 10 random images from each slide were blindly analyzed. The percentage of $ki67^+$ hCMs was counted as the number of $ki67^+$ hCMs dividing total cTnT positive cells.

2.19. Scanning electron microscope (SEM) analysis

The SIS and cell-seeding SIS patches were fixed with 2.5% glutaraldehyde at 4 °C overnight, then they were rinsed in 0.1 M phosphate buffer (pH 7.3) 10 min for 3 times and post fixed in 1% osmium tetroxide for 1 h at room temperature. The samples were rinsed 3 times with the same buffer before gradient dehydration with ethanol and drying in

critical point microenvironment without surface tension. Finally, the samples were coated with gold and examined on a FEI Quanta250 scanning electron microscope as previously described [45].

2.20. Protein extraction and liquid chromatography-tandem mass spectrometry (LC-MS/MS) analysis

For sample preparation, the CdM from hCVPCs, hCMs, and Mix (2×10^6 cells each) was collected using serum-free DMEM after incubation for 48 h. Then, a total of 6 mL supernatant from each CdM (CdM-supernatant) was collected after removing cells debris by centrifuge in 10000 *g* at 4 °C for 20 min (Hitachi CR21G), and 4 μL all protease inhibitor (Pierce™, Thermo Fisher Scientific) was added to protect proteins from degradation. For protein extraction and tryptic digestion, a 4-fold volume of acetone was added to the CdM-supernatant and kept in −20 °C for 10 h. Subsequently, the acetone-precipitated proteins were washed three times with cooled acetone. The dried acetone-precipitated proteins were used for protein digestion by Filter-aided sample preparation (FASP) procedure. The proteins were resuspended in 200 μL 8 M urea (pH 8.0). The protein concentrations were determined using Bradford method (Eppendorf Biospectrometer) in accordance with the manufacturer's protocol. Then proteins were loaded in 10 kD Microcon filter tubes (Sartorius) and centrifuged at 12,000 g for 20 min. The precipitate in the filter was washed two times by adding 200 μL 50 mM NH_4HCO_3. The precipitate was resuspended in 100 μL 50 mM NH_4HCO_3. Protein samples underwent trypsin digestion (enzyme-to-substrate ratio of 1:50 at 37 °C overnight) in the filter, and then were collected by centrifugation at 12,000 g for 15 min. Additional washing, twice with 200 μL of MS water, was essential to obtain greater yields. Peptides were dried with SpeedVac (Eppendorf).

Then, digested peptides were analyzed on a Q Exactive HF-X mass spectrometer coupled with Easy-nLC 1200 system (both Thermo Fisher Scientific). Raw files were searched against the human RefSeq protein database (version July 04, 2013) with Proteome Discoverer (Thermo Fisher Scientific, version 2.3.0) using the MASCOT search engine [46]. The amount of each gene product was estimated with a label-free, intensity-based absolute quantification (iBAQ) approach as we previously reported [47]. Fraction of total (FOT) is a relative quantification value defined as a protein's iBAQ divided by the sum of the iBAQ of all proteins identified in an experiment, calculated as the normalized abundance of a particular protein in the experiment. For the ease of presentation in the subsequent analysis, the FOT was further multiplied by 1e5. The bioinformatics analyses were performed using the Database for Annotation, Visualization and Integrated Discovery (DAVID) Bioinformatics Resource (http://david.abcc.ncifcrf.gov/).

2.21. Statistical analysis

Data are presented as mean ± SEM. Statistical significance was analyzed by using the unpaired Student's *t*-test for engraftment and *in vitro* comparation between two groups and paired *t*-test for LVEF, LVFS, LVEDD, and LVESD analysis (intra-group) or one-way analysis of variance (ANOVA) followed with Bonferroni's multiple as appropriate (histological, RT-qPCR, or *in vitro* results). Two-way ANOVA was applied with Tukey's multiple comparison for analysis of echocardiographic data (LVEF, LVFS, LVESD, and LVEDD). Statistical analyses were illustrated with GraphPad Prism 6.1. A p value < 0.05 was considered statistically significant.

3. Results

3.1. Characterization of hiPSCs, hCVPCs, and hCMs

The hiPSCs were engineered with CRISPR/Cas9 system to carry GFP (Fig. S1A). The immunocytochemical staining and flow cytometry analysis confirmed the robust expression of GFP (Fig. S1B and C) and high ALP activity (Fig. S1D) in these hiPSCs. The flow cytometry analysis showed that ~99% of the hiPSCs expressed a pluripotency marker SSEA4 (Fig. S1E) and the immunocytochemical staining revealed the uniform expression of pluripotency markers OCT4, SSEA4, and NANOG in the hiPSCs (Fig. S1F).

The hiPSCs were then induced to generate $SSEA1^+$ hCVPCs and hCMs respectively, following the methods reported previously [32–34,48]. The immunocytochemical staining showed that the hCVPCs displayed hCVPC markers GATA4, MESP1, ISL1, and NKX2-5 (Fig. S2A). FACS analysis confirmed a high cell population expressing SSEA1 (93.1%–94.7%) (Fig. S2B) as reported previously [4,12,32,38]. The hCMs displayed cardiomyocyte markers cTnT and α-actinin (Fig. S2C). The FACS analysis further confirmed that the majority of cells expressed cTnT (Fig. S2D).

3.2. The SIS patch supports the growth of hCVPCs and hCMs

hCVPCs, hCMs, or Mix ($3 \times 10^5/cm^2$ each) were seeded onto the SIS patch at a thickness ~80–100 μm in a size 9 mm in length and 5 mm in width (Fig. 1A). After cultivated for 24-h, the attachment of these cells on the SIS patches was observed by a fluorescence microscopy (Fig. 1B). The viability of hCVPCs, hCMs, and Mix on the SIS patches was significantly improved compared with these on the 96 well culture plates analyzed by CCK-8 assay (Fig. 1C). Moreover, the cell number of hCVPCs and hCMs both increased after cultivated on the SIS patches (Fig. S3A). Flow cytometry analyses further showed a higher population of $Ki67^+$ hCVPCs on the SIS patches than that on the plate (Fig. S3B), while the populations of $Ki67^+$ hCMs were similar between the two groups (Fig. S3C). Therefore, the enhanced cell viability in the SIS-hCVPC group is at least related to the improved proliferation of hCVPCs, while the enhanced cell viability in the SIS-hCM group seems mainly related to the improved cell survival of hCMs. The collagen fiber bundle in the SIS patch intertwined into a 3D network-like structure and the seeding cells adhered and stretched between/on the collagen fibers of the SIS patch observed by the SEM (Fig. 1D). Moreover, FACS analyses showed that the hCVPCs (Fig. 1E), hCMs (Fig. 1F), and Mix (Fig. 1G) on the SIS patch maintained high purity with the expression of SSEA1 and/or cTnT, respectively. Further, the hCM on the SIS patch began to beat synchronously with the entire SIS after two days cultivation (Video S2), indicating that the hCMs are functional and connected with the SIS patches. To observe the morphology of cells seeded on the SIS patch more clearly, hCVPCs were seeded at a low density of $1 \times 10^4/cm^2$ and hCMs or Mix were seeded at a density of $5 \times 10^4/cm^2$. The hCVPC markers (MESP1 and GATA4) and the cardiomyocyte markers (cTnT and α-actinin) were universally detected in the SIS patches with hCVPCs (Fig. S4A) and hCMs (Fig. S4B), respectively. The MESP1- or ISL1-expressing hCVPCs and cTnT- or α-actinin-expressing hCMs were detected in the SIS-Mix patches (Fig. S4C).

Supplementary video related to this article can be found at https://doi.org/10.1016/j.bioactmat.2023.05.015

3.3. Comparison of heart function and cell retention between intramyocardial injection of hCVPCs and epicardial implantation of SIS-hCVPC patches

We then compared the heart function and cell retention between the intramyocardial injection of hCVPCs and epicardial implantation of SIS-hCVPC patches with the same cell dose (2×10^5) in the MI mice. The echocardiography analysis showed that both hCVPC-injection and SIS-hCVPC patches reversed worsening LVEF and inhibited decline of LVFS induced by MI, while the SIS-hCVPC patches showed better improvements in LVEF and maintenance of LVFS than the hCVPC-injection (Fig. S5A and B). Consistently, higher levels of hGAPDH and more GFP^+ cells were detected in the hearts treated with the SIS-hCVPC patches than these treated with the hCVPC-injection within the 72 h post-implantation (Fig. S5C and D).

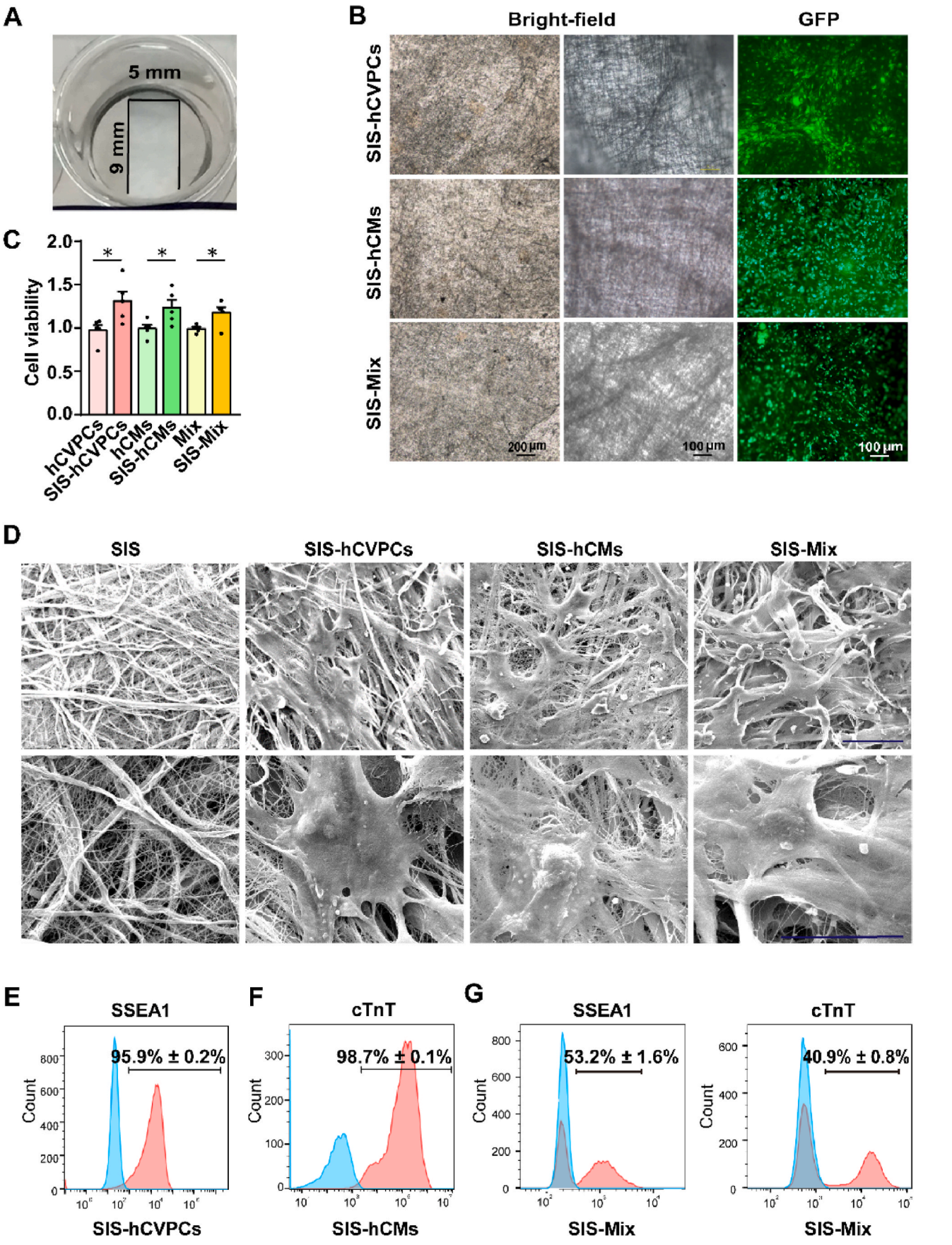

(caption on next page)

Fig. 1. Generation and characterization of hiPSC-derived cardiac lineage cell-seeding SIS patches. **(A)** Photographic image of the small intestinal submucosa (SIS) patch in a culture dish. **(B)** Images of hCVPCs, hCMs, and the Mix (hCVPCs: hCMs, 1:1) seeding on the SIS patch at a cell density of $3 \times 10^5/cm^2$ obtained under a bright-field (left panel, at low magnification, middle panel, at high magnification) and fluorescence (right panel) microscopy. **(C)** Analyses of cell viability of hCVPCs, hCMs, and Mix cultivated on the SIS patches or without the patches by using the Cell Counting Kit-8 (CCK-8) assay. n = 5. Data are mean ± SEM. Statistical significance was assessed using *t*-test. $*p < 0.05$. **(D)** Images of the SIS, SIS-hCVPCs, SIS-hCMs, and SIS-Mix obtained from scanning electron microscope. Scar bars, 50 μm. **(*E*–G)** Flow cytometry analysis of $SSEA1^+$ (hCVPC marker) and $cTnT^+$ (cardiomyocyte marker) populations of the hCVPCs (**E**), hCMs (**F**), and Mix (**G**) seeded on the SIS patches. The blue filled histogram, isotype control; and the red filled histogram, the positive population. n = 3 each.

3.4. hiPSC-derived cardiac lineage cell-seeding SIS patches improve cardiac function and reduce LV dilation of infarcted hearts

To determine effects of mono cell- and dual cell-seeding SIS patches in cardiac repair, we compared the functional outcome at day 7 post-MI just before the implantation and at day 28 post-implantation (i.e., day 35 post-MI) (Fig. 2A). The survival rate of mice within 28 days post-implantation did not show significant difference (4 deaths of 25 in MI Ctrl, 3 deaths of 23 in SIS, 1 death of 24 in SIS-hCVPCs, 1 death of 20 in SIS-hCMs, and 1 death of 22 in SIS-Mix) among each group (Fig. 2B). The induction of MI by LAD ligation was confirmed by echocardiography (Fig. 2C) and ST-elevations (Fig. S6A), followed by the inversion of Q waves and T-waves at day 7 post-MI and 30 min post-implantation recorded by electrocardiogram (Fig. S6B). The MI induced comparable reductions in LVEF and LVFS as well as enhanced LVESD and LVEDD at day 7 post-MI in all groups before the implantation (Fig. 2D, E and F; Fig. S7). No arrhythmic events were record during the 30 min after cell implantation (Fig. S6B). By day 28 post-implantation, the MI control animals showed a significant decline in LV function (−20% in LVEF, $p < 0.0002$ and −21.9% in LVFS, $p < 0.0001$) and ventricular dilation (+15.1% in LVEDD, $p < 0.0001$ and + 20.8% in LVESD, $p < 0.0001$) relative to their baseline values at 7 days post-MI (Fig. 2D, E and F; Fig. S7A and B). The LVEF and LVFS but not LVESD and LVEDD showed a tendency of slight improvements in the SIS group compared with the MI Ctrl group (Fig. 2D), but the LV function remained significant decline with the ventricular dilation relative to their baseline values (Fig. 2E and F; Fig. S7A and B). However, the cardiac function and LVESD at day 28 post-implantation were preserved in all cell-seeding SIS groups compared with these in the MI Ctrl and SIS groups (Fig. 2D, E and F; Fig. S7A and B). Notably, the animals receiving the SIS-Mix showed enhanced cardiac function and reversed the progress of LV dilation relative to their baseline values, and had better therapeutic effects compared with the SIS group (Fig. 2D, E and F; Fig. S7A and B). Taken together, these results demonstrate that implantation of the SIS alone has a minor beneficial effect in the improvement of LV function, whereas the hCVPC- and hCM-seeding SIS patches lead to significant improvements of cardiac function and LV dilation at the end-systole; and the dual hCVPC- and hCM-seeding SIS patches have better benefits for the restoration of myocardial performance and prevention of ventricular dilation.

3.5. hiPSC-derived cardiac lineage cell-seeding SIS patches reverse pathological ventricular remodeling of infarcted hearts

We next assessed the influence of the SIS with and without cells in the pathological ventricular remodeling. All MI animals showed scar formation and collage deposition at 35 days post-MI (Fig. 3A and B). Notably, the scar sizes in the SIS-hCVPC, SIS-hCM, and SIS-Mix groups were significantly smaller than these in the MI Ctrl group, while the SIS group only showed a reduction tendency (Fig. 3A). Consistent with the better improvement in the cardiac function, the SIS-Mix group exhibited significant reduction of scare formation compared with the SIS group (Fig. 3A). RT-qPCR analysis showed increases of transcript levels of *Col1* and *Col3* in the LV at 35 days post-MI, whereas they were downregulated by the SIS and SIS-cell patches (Fig. S8A). Moreover, the SIS-Mix patches had the stronger inhibition in the *Col1* expression than the SIS-hCVPC ones (Fig. S8A). Further, the collagen fibers stained with picrosirius red were observed with polarized light (thicker fibers exhibit red-orange (type I collage) and thinner fibers appear green (type III collage) (Fig. 3B). In the infarct and border zones, the thicker fibers were significantly decreased in the SIS-hCM and SIS-Mix groups but not the SIS-hCVPC one compared with these in the SIS group; and the thinner fibers were increased in the SIS-hCM and SIS-Mix but not the SIS-hCVPC groups compared with these in the MI Ctrl and SIS groups (Fig. 3C). Therefore, the ratios of collagen III/I fibers in the infarct and border zones were comparable among the MI Ctrl, the SIS, and the SIS-hCVPC groups, while they were significantly increased in the SIS-hCM and SIS-Mix groups (Fig. S8B). Moreover, the cross-sectional areas of cardiomyocytes in the infarcted hearts implanted with SIS and SIS-cell patches were significantly smaller than these in the MI Ctrl group, and the cross-sectional area of cardiomyocytes in the SIS-Mix group was smaller than that in the SIS group (Fig. 3D). This was further confirmed by RT-qPCR analysis showing that the transcript levels of hypertrophic marker genes *Anp*, *Bnp,* and *Myh6* in the LV were significantly increased at 35 days post-MI, whereas they were downregulated by the SIS and SIS-cell patches (Fig. S9). Notably, the inhibitory effects of SIS-Mix patches in the expression of *Anp* and *Bnp* were stronger than the SIS and SIS-hCVPC patches (Fig. S9). These results demonstrate that the SIS patch alone is not enough to prevent fibrosis formation, though it ameliorates myocardial hypertrophy, whereas the SIS-cell patches significantly suppress fibrosis formation and improve myocardial remolding and the SIS-hCM and SIS-Mix patches are more effective in enhancing the ratio of collagen III/I fibers compared with the SIS and SIS-hCVPC patches. Moreover, the dual cell patches are more effective in the suppression of cardiomyocyte hypertrophy compared with the SIS patches.

3.6. hiPSC-derived cardiac lineage cell-seeding SIS patches promote cardiomyocyte proliferation and angiogenesis in the infarcted hearts

One of fundamental goals of cell-based cardiac therapies is to compensate cardiomyocyte loss with one strategy to stimulate host cardiomyocytes to re-enter cell cycle and proliferate. We thus investigated whether the promoted healing of infarcted hearts mediated by hPSC-cardiac lineage cell-seeding SIS patches is associated with the increases in cell-cycle activity and proliferation of host cardiomyocytes. The cardiomyocytes in the infarcted hearts at 35 days post-MI were evaluated by fluorescent immunohistochemistry analyses for cell-cycle progression via PH3 expression (a marker of late G2 phase/mitosis), for proliferation via Ki67 expression, and for cytokinesis via Aurora B expression. The MI Ctrl and SIS groups showed comparable number of $PH3^+$ and $Ki67^+$ cardiomyocytes in the border zone, while more $PH3^+$ and $Ki67^+$ cardiomyocytes were detected in the hearts from all SIS-cell groups than these in the MI Ctrl and SIS groups (Fig. 4A and B). Moreover, the number of $PH3^+$ and $ki67^+$ cardiomyocytes in the SIS-Mix group was significantly higher than these in the SIS-hCVPC and SIS-hCM groups (Fig. 4A and B). Consistently, the frequency of cardiomyocytes expressing Aurora B was similar between the MI Ctrl and SIS groups, while it was significantly enhanced in all SIS-cell groups compared with these in the MI Ctrl and SIS groups and was the highest in the SIS-Mix group (Fig. 4C). In addition, the fluorescent immunohistochemistry analysis revealed increases in the number of $CD31^+$ (Fig. 5A) and α-SMA^+ (Fig. 5B) vessels in both infarct and border zones of the hearts treated with the SIS alone. The beneficial effect in promoting vascularization was further enhanced by the SIS-cell patches. Particularly, the number of $CD31^+$ vessels in the border zone of the hearts

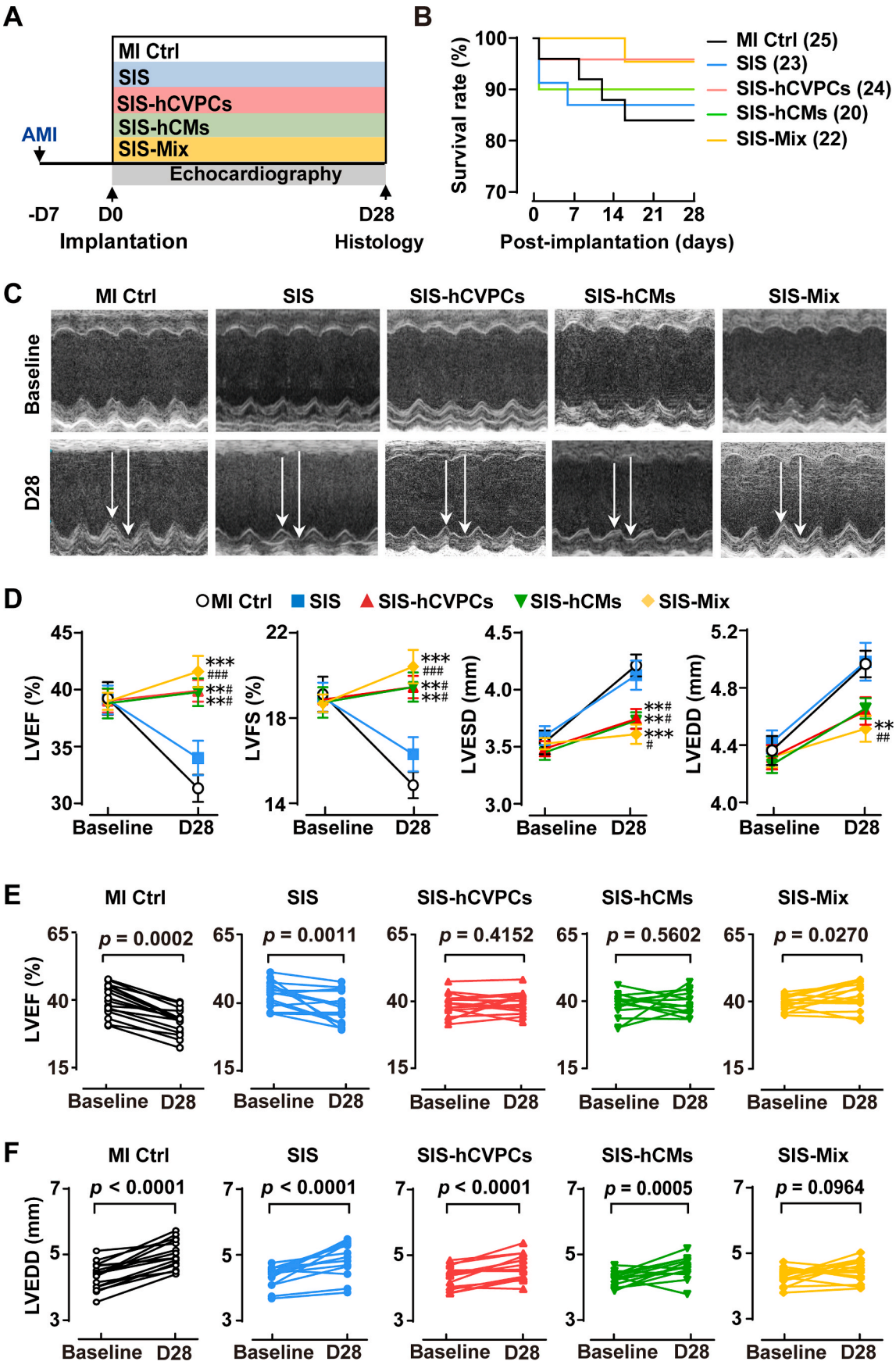

(caption on next page)

Fig. 2. Cell-seeding SIS patches promote functional recovery of murine infarcted hearts. **(A)** Schematic of study design and the data collection time for echocardiographic analysis. All animals received cyclosporine A from one day before-to day 7 post-implantation. AMI, acute myocardial infarction; MI Ctrl, MI Control. **(B)** Kaplan–Meier survival curves for MI mice. **(C)** Representative M-mode images of echocardiography hearts from various groups at day 7 post-MI before the implantation (baseline) and day 28 post-implantation (D28). **(D)** Echocardiographic analysis of LV function (LVEF, LVFS) and dilation (LVESD, LVEDD). n = 13–16 for each group. All values were mean ± SEM. Two-way ANOVA was used for statistical analyses. $^{**}p < 0.01$, $^{***}p < 0.001$ vs. the MI Ctrl group; $^{\#}p < 0.05$, $^{\#\#}p < 0.01$, $^{\#\#\#}p < 0.001$ vs. the SIS group. **(E–F)** LVEF **(E)** and LVEDD **(F)** at baseline (day 7 post-MI before the implantation) and D28 post implantation. n = 13–16 for each group. A paired *t*-test for comparison of cardiac function within groups between baseline and 28-day follow up.

treated with SIS-hCM patches (Fig. 5A) and the number of α-SMA$^+$ vessels in the infarct and border zones of the hearts treated with the SIS-cell patches (Fig. 5B) were higher than that in the SIS alone group. Meanwhile, the α-SMA$^+$ vessels were detected sprouting into the engrafted SIS patches with and without seeded cells (Fig. 5C, left panels), whereas more vascularity was detected in the engrafted SIS-cell patches than that in the SIS patches alone (Fig. 5C, right panel). In addition, besides α-SMA$^+$ vessels detected, a small portion of co-expressing GFP$^+$ α-SMA$^+$ vessels were comparably detected in the engrafted SIS-hCVPC and SIS-Mix patches (Fig. 5D), suggesting the vascularity in the engrafted patches are formed from both host arterioles and hCVPC-derived vasculogenesis. Furthermore, the red blood cells were observed inside the α-SMA$^+$ blood vessel in the SIS-Mix patch (Fig. 5E, left 3 panels) and the intact α-SMA$^+$ blood vessel was interspersed from the host myocardium to the SIS-Mix patch (Fig. 5E, right 2 panels), suggesting a possible connection of the arterioles in the engrafted patches with these in the cardiac myocardium. Collectively, these results suggest that the increases in the cell-cycle activation and proliferation of host cardiomyocytes as well as the angiogenesis in the host hearts and engrafted patches might partially attribute to the therapeutic effects of hPSC-derived cardiac lineage cell-seeding SIS patches in the infarcted hearts.

3.7. hiPSC-derived cardiac lineage cell-seeding SIS patches have long-term therapeutic effects in the infarcted hearts

One of the major challenges for cell therapy is the diminishment of beneficial effects [3,13,49]. To investigate this, we examined cardiac function at 90 days post-implantation (Fig. 6A). Echocardiography analysis showed that all groups exhibited comparable LV function and ventricular diameter at day 7 post-MI (Fig. 6A). The LVEF, LVFS, and LVESD were continuously worsened at 90 days post-MI, however, the LV function but not LVESD were significantly improved in the SIS group (Fig. 6A). Notably, the preserved cardiac function and reduced LVESD seen at 28 days post-implantation in all cell-seeded SIS groups (Fig. 2) were sustained for 90 days and the significantly better cardiac function was observed in the SIS-Mix group than that in the SIS group (Fig. 6A). Consistently, the scar size was smaller in all SIS-cell groups than that in the MI Ctrl one, while it did not show statistical significance between the SIS and MI Ctrl groups (Fig. 6B). In addition, more α-SMA$^+$ vessels were detected in the SIS alone and all SIS-cell groups than that in the MI Ctrl one (Fig. S10). Taken together, these results reveal that the cell-seeding SIS patches are able to restore the declined myocardial function and reduce ventricular dilation at the end of contraction with the smaller fibrotic scar at 90 days post-implantation. Particularly, the improvement of cardiac function in the SIS patch seeded with dual hCVPCs and hCMs is better than that in the SIS alone.

3.8. Dual hiPSC-derived cardiac lineage cell-seeding SIS patches increase long-term cell retention and integration

The low rate of cell retention hampers the efficacy of cell therapy [50,51]. We then assessed whether better therapeutic effects seen in the dual cell-seeding SIS patches are accompanied with the improvement of cell retention and integration. The implanted SIS patches visually became thinner and merged with the host hearts over time (Fig. S11A). Then they were invaded by host cells and sprouted with α-SMA$^+$ vessels at 28 days post-implantation, and hardly separated from the native tissue at 90 days post-implantation (Fig. S11B). To trace the implanted GFP$^+$ cells, the GFP antibody was detected by the FITC-conjugated secondary antibody as the auto-fluorescence of GFP in the cells on the SIS patches was greatly decreased after fixed with 4% PFA (Fig. S12A) and omitting the primary antibody was used as a control (Fig. S12B). At 28 days post-implantation, no GFP signal was detected in the MI Ctrl and SIS groups (Fig. S12C), while more GFP$^+$ cells were observed in the SIS-hCVPC and SIS-Mix groups than these in the SIS-hCM group (Fig. 6C), though the detected GFP$^+$ cells were only around 0.30–8.80 ten-thousandth of implanted cells. At 90 days post-implantation, the GFP$^+$ cells were only observed in the sections of SIS-hCVPC and SIS-Mix groups but hardly detected in the SIS-hCM group. In addition, more GFP$^+$ cells were observed in the SIS-Mix group than these in the SIS-CVPC one (Fig. 6C). Notably, a small proportion of GFP$^+$ cTnT$^+$ cells were detected both in the border and infarct zones and GFP$^+$ α-SMA$^+$ arterioles were also observed in the host infarcted hearts beyond the epicardial layer up to 90 days in both SIS-hCVPC and SIS-Mix groups (Fig. 6D, representative images), which indicates the possible migration of implanted cells seeded on the SIS into the host hearts or the integration with the host myocardium. Interestingly, the number of cells co-expressing α-SMA and GFP in the host hearts was similar in the two groups, while more GFP$^+$-cTnT$^+$ cardiomyocytes in the SIS-Mix group were lining up alone the treated region compared with these in the SIS-hCVPC group (Fig. 6D). Thus, the small proportion of implanted cells appear to incorporate to the native vessels and cardiomyocytes. Moreover, the results suggest that the combination of hCVPCs with hCMs enhances the integration of implanted cells with the host myocardium.

3.9. Paracrine activity from the cell-seeding SIS patches contributes to the enhanced cardiomyocyte proliferation and tube formation

Next, we studied whether the enhanced proliferation of cardiomyocytes and vascularization by cell-seeding SIS patches is related to the paracrine activity by examining the effects of the conditioned media (CdM) from the SIS and cell-seeding SIS patches in these cells. Consistent with the *in vivo* data (Fig. 4B), treatments of cardiomyocytes with the CdM from the SIS-cell patches but not the SIS patches increased the number of Ki67$^+$ cardiomyocytes relative to the one in the DMEM control group (Fig. 7A). More Ki67$^+$ cardiomyocytes were detected in the CdM from the SIS-Mix group than that in the SIS-hCVPC-CdM and SIS-hCM-CdM groups (Fig. 7A). These results suggest that the paracrine effect from the cells but not the SIS contributes to the enhanced proliferation of cardiomyocytes. For the tube formation of HUVECs, treatments of HUVECs with the CdM from the SIS-cell but not the SIS patches significantly increased the total branching length of the cells compared with that in the DMEM control group (Fig. 7B), indicating paracrine activity of the cells on the SIS patches is involved in the enhanced angiogenesis. The wound healing assays in the HUVECs showed similar enhancement of healing process between the CdM from the SIS- and SIS-cell-patches compared with the DMEM control group (Fig. 7C). Therefore, the promoted migration of ECs seems mainly from the paracrine activity of the SIS patches.

3.10. Co-cultivation of hCVPCs and hCMs alters the secretome of each cell types

Then we compared the secretome of these cells and explored whether

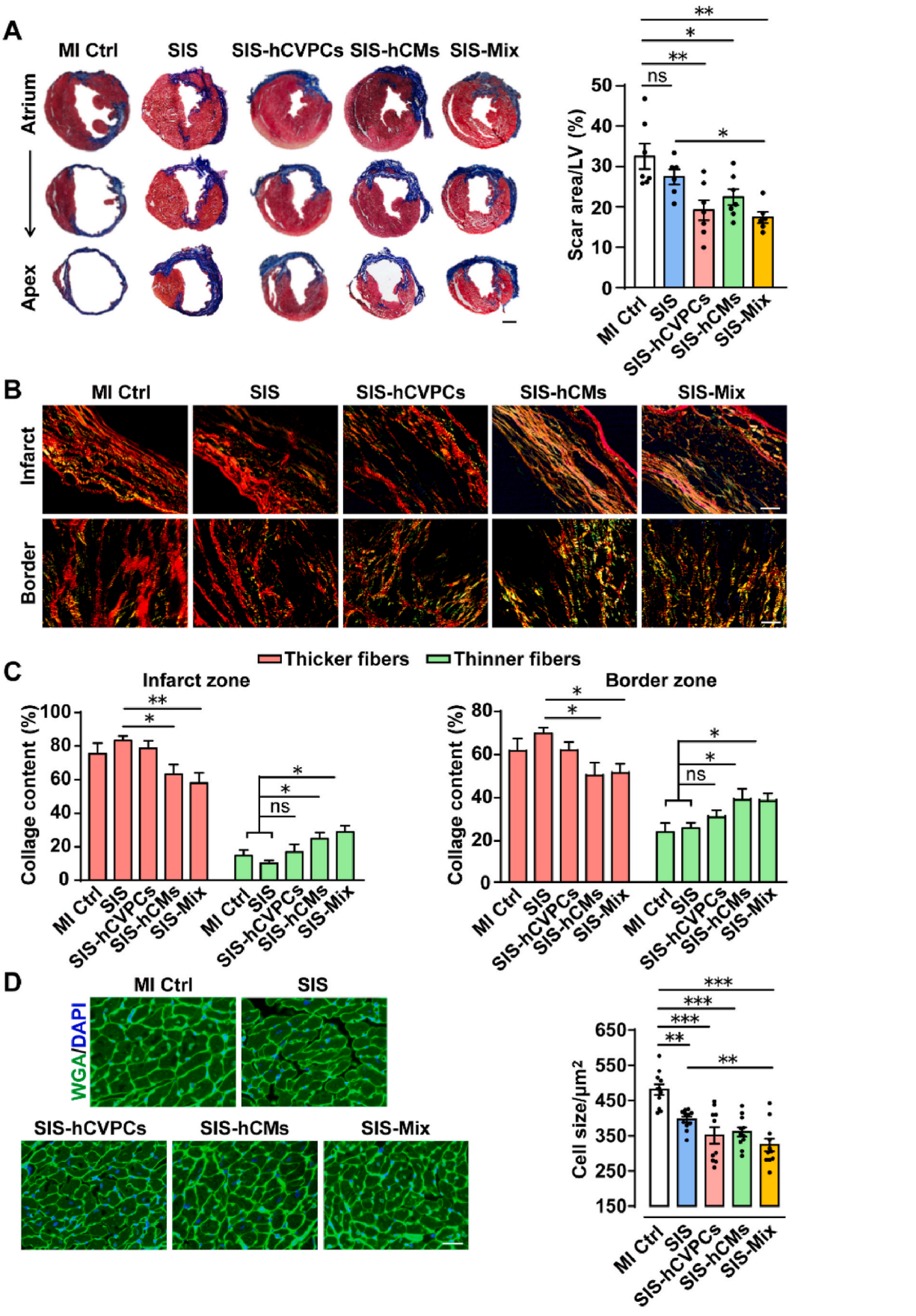

(caption on next page)

Fig. 3. Cell-seeding SIS patches ameliorate pathological ventricular remodeling at 28 days post-implantation. **(A)** Representative images of infarcted mouse heart sections stained with Masson-trichome and quantification of scar areas. Scale bar, 1 mm. **(B)** Representative photomicrographs with polarized light (magnification, 20×) of the infarct and border zones stained with picrosirius red. Thicker fibers exhibit red-orange birefringence (type I collage), whereas thinner fibers appear green (type III collage). Scale bar, 50 μm. **(C)** Percentages of type I (red-orange) or III (green) collagen fibers to the total amount of collagen fibers in the infarct and border zones. **(D)** Representative images and quantification of wheat germ agglutinin (WGA) stained cardiomyocytes from the same part of the infarct myocardium. Scale bar, 50 μm. n = 6–7 hearts for each group. MI Ctrl, MI control. All values were mean ± SEM. One-way ANOVA was used for statistical analyses. $^{*}p < 0.05$, $^{**}p < 0.01$, $^{***}p < 0.001$; ns, no statistical significance.

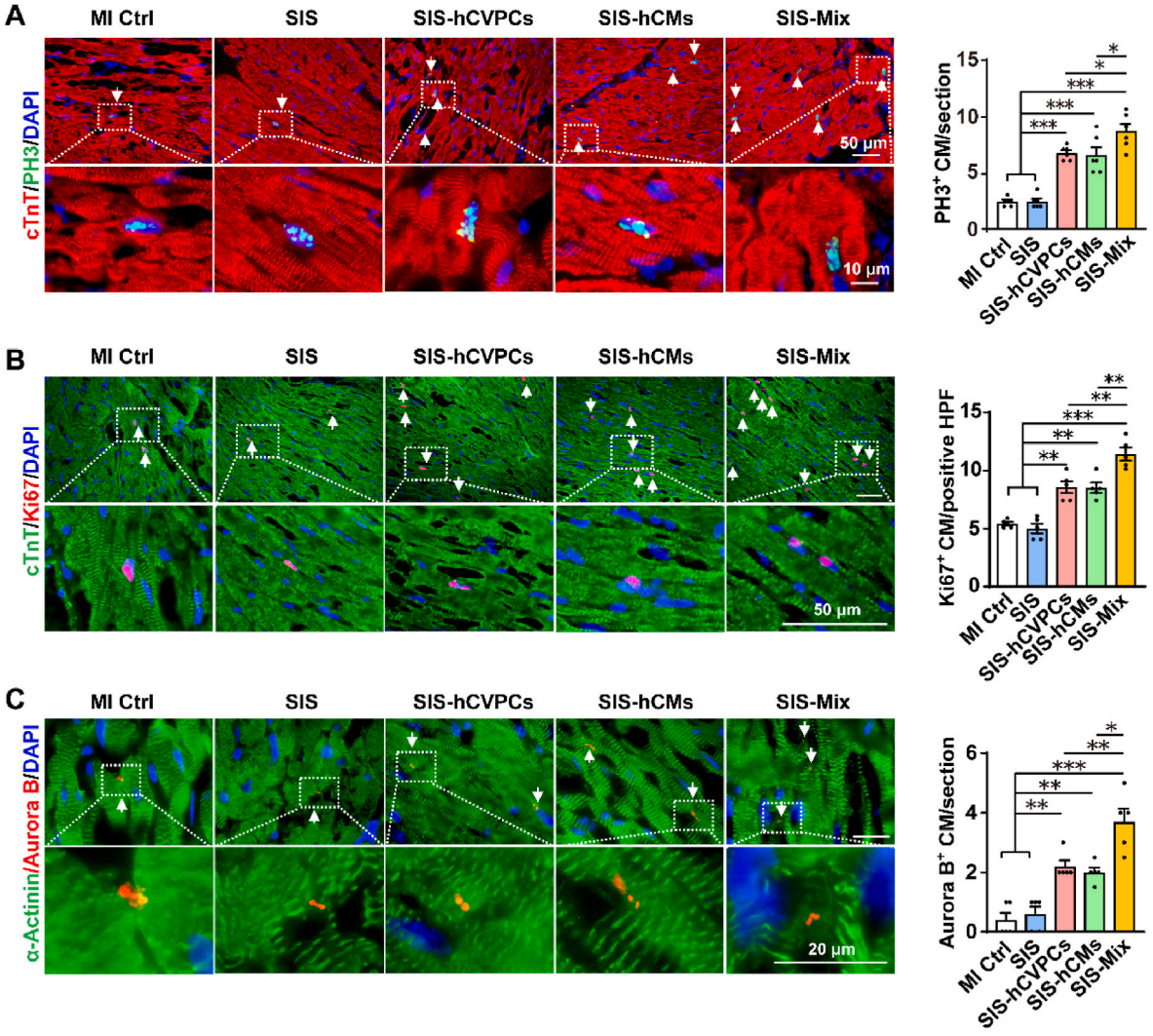

Fig. 4. Implantation of cell-seeding SIS patches promotes cardiomyocyte proliferation in the infarcted hearts. **(A–C)** Representative images and quantification of co-fluorescent immunohistochemistry staining for cTnT and α-actinin with $PH3^{+}$ **(A)**, $Ki67^{+}$ **(B)**, and Aurora kinase B^{+} (Aurora B^{+}) **(C)** cardiomyocytes in the border zone of heart sections collected at day 28 post-implantation. The white arrows indicated positive cells. MI Ctrl, MI control; HPF, per high-power field. n = 6–7 hearts each in **(A)** and **(B)**; n = 5 hearts each in **(C)**. All values were mean ± SEM. One-way ANOVA was used for statistical analyses. $^{*}p < 0.05$, $^{**}p < 0.01$, $^{***}p < 0.001$.

the interaction of hCVPCs and hCMs induces extra paracrine factors, which might contribute to the better therapeutic effects for infarcted hearts compared with these from the mono-cell type. The LC-MS/MS-based in-depth proteomic analysis of the secretory proteins was performed using the CdM collected from the equal number of hCVPCs, hCMs and their 1:1 mixture. Then the label-free quantification of MS data and statistical analyses were used to compare the three groups. The venn diagram showed that more proteins were detected in the Mix-CdM group than these in the hCVPC-CdM and the hCM-CdM: a total of 1653 proteins in the Mix-CdM, 819 proteins in the hCVPC-CdM and 769 proteins in the hCM-CdM (Fig. 8A). Among these proteins, 431 proteins were shared among three groups, 11 proteins were shared between the hCVPC-CdM and the hCM-CdM, and more proteins were shared between the Mix-CdM and the hCVPC-CdM (287) or the hCM-CdM (250). Strikingly, only about 10%–11% of proteins in the hCVPC-CdM and the hCM-CdM were exclusively expressed, whereas about 41% of proteins (685) in the Mix-CdM were exclusively expressed (Fig. 8A). The shared proteins among three groups were annotated for Gene Ontology Biological Process (GOBP). Consistent with our functional data demonstrating that SIS-cell patches reduced fibrosis, promoted cell proliferation and angiogenesis in infarcted hearts, the proteomic analysis indicated that their secretomes were actively involved in cell adhesion, ECM organization, anti-cell apoptosis, cell migration, cell growth, angiogenesis, and wound healing (Fig. 8B). GOBP analysis of the unique proteins detected in the hCVPC-CdM and hCM-CdM showed distinct paracrine effects between them: the specific proteins detected in the hCVPC-CdM were

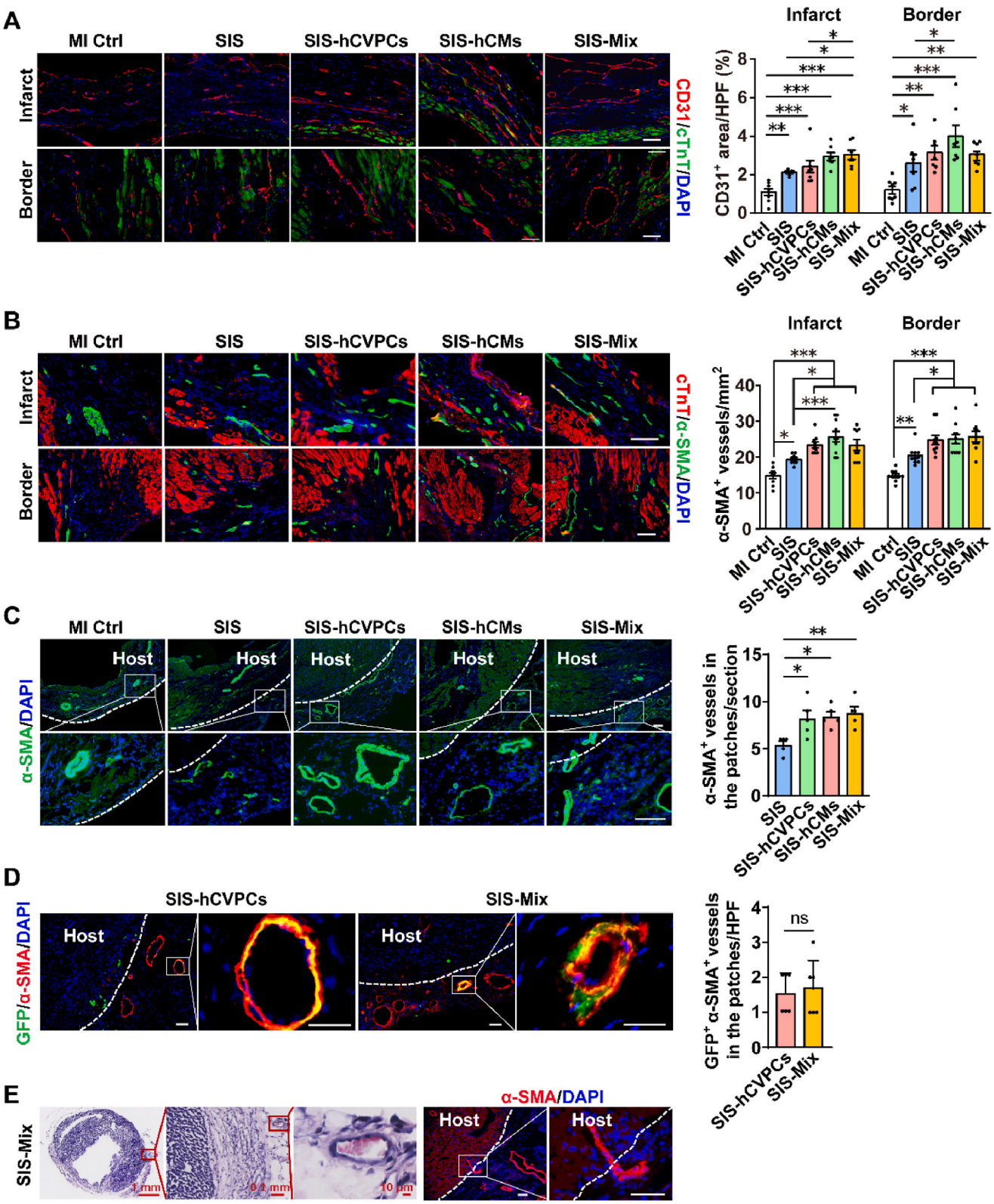

Fig. 5. Implantation of cell-seeding SIS patches significantly enhance vascularization of the infarcted hearts. **(A–B)** Representative images and quantification analysis of co-fluorescent immunohistochemistry staining for cTnT and DAPI with $CD31^+$ areas **(A)** and α-SMA^+ blood vessels **(B)** in the infarct and border zones of heart sections collected at 28 days after implantation. n = 6–7 hearts each. **(C)** Representative images and quantification analysis of fluorescent immunohistochemistry staining for DAPI with α-SMA^+ blood vessels in the hearts with or without engrafted patches. **(D)** Representative images and quantitative analysis of hCVPCs-derived vasculogenesis in the engrafted SIS-hCVPC and SIS-Mix patches by fluorescent immunohistochemistry staining for GFP and α-SMA. **(E)** The integration of blood vessels in the SIS-cell patches with the host myocardium. (Left 3 panels) Low- and high-magnification images of the SIS-Mix patch-treated heart section stained with α-SMA and counterstained with H&E showing presence of red blood cells indicative of blood perfusion. (Right 2 panels) Representative images of immunohistochemistry staining for α-SMA. Scar bar, 50 μm. n = 4–5 hearts each. MI Ctrl, MI Control. HPF, per high-power field. All values were mean ± SEM. One-way ANOVA was used for (A), (B), and (C); unpaired *t*-test was used for (D). $^*p < 0.05$, $^{**}p < 0.01$, $^{***}p < 0.001$; ns, no statistical significance.

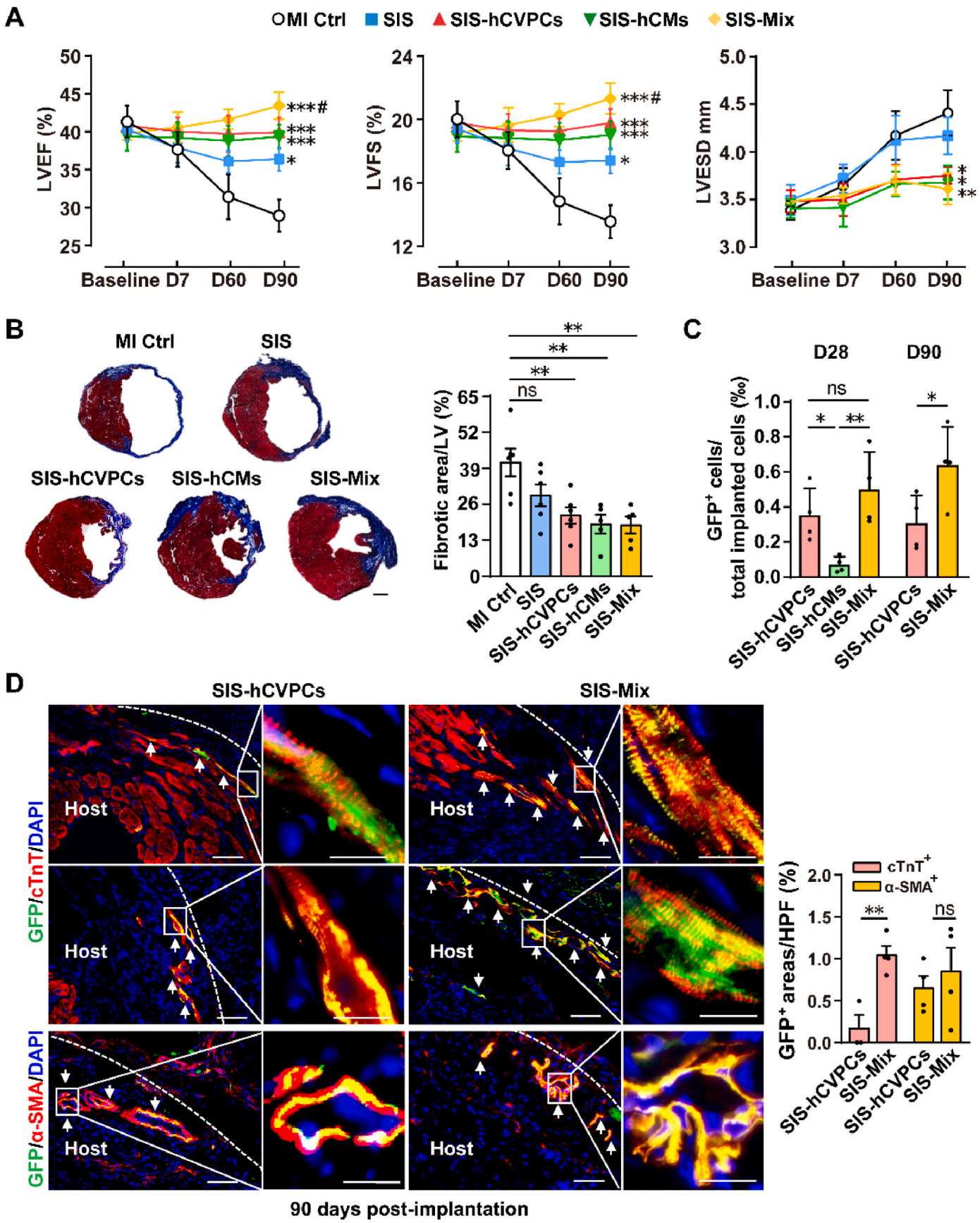

(caption on next page)

Fig. 6. Implantation of cell-seeding SIS patches exert long-term therapeutic effects for infarct hearts. (A) Echocardiography analysis of LV function at pre-implantation (day 7 post-MI, baseline) and day 7, 60, and 90 follow-ups. n = 6–7 each. Two-way ANOVA was used for statistical analyses. $^{*}p < 0.05$, $^{**}p < 0.01$, $^{***}p < 0.001$ vs. the MI control group (MI Ctrl); $^{\#}p < 0.05$ vs. the SIS group. **(B)** Representative images and quantitative analysis of heart sections stained with Masson's trichrome at day 90 post-implantation. Scale bar, 1 mm. n = 5–6 each. **(C)** Quantification of the GFP^{+} cells in the hearts at 28 days and 90 days post-implantation. The total number of nuclei for both GFP and DAPI signals in two heart sections and from same layers were calculated and divided by the total number of implanted cells (2×10^5). n = 4 each. **(D)** Engrafted cells were tracked by fluorescent immunohistochemistry staining for GFP^{+} cells co-stained with cTnT (upper panels for border zones and middle panels for infarct zones) or α-SMA (lower panels) and counterstained nuclei with DAPI in the infarcted myocardium at day 90 post-implantation. The white arrows indicated GFP^{+} cells. Scale bar, 50 μm (left panels) and 20 μm (right panels) in each group. HPF, per high-power field. n = 4 hearts each. All values were mean ± SEM. One-way ANOVA was used for (B) and (C, D28); unpaired *t*-test was used for (C, D90) and (D). $^{*}p < 0.05$, $^{**}p < 0.01$; ns, no statistical significance.

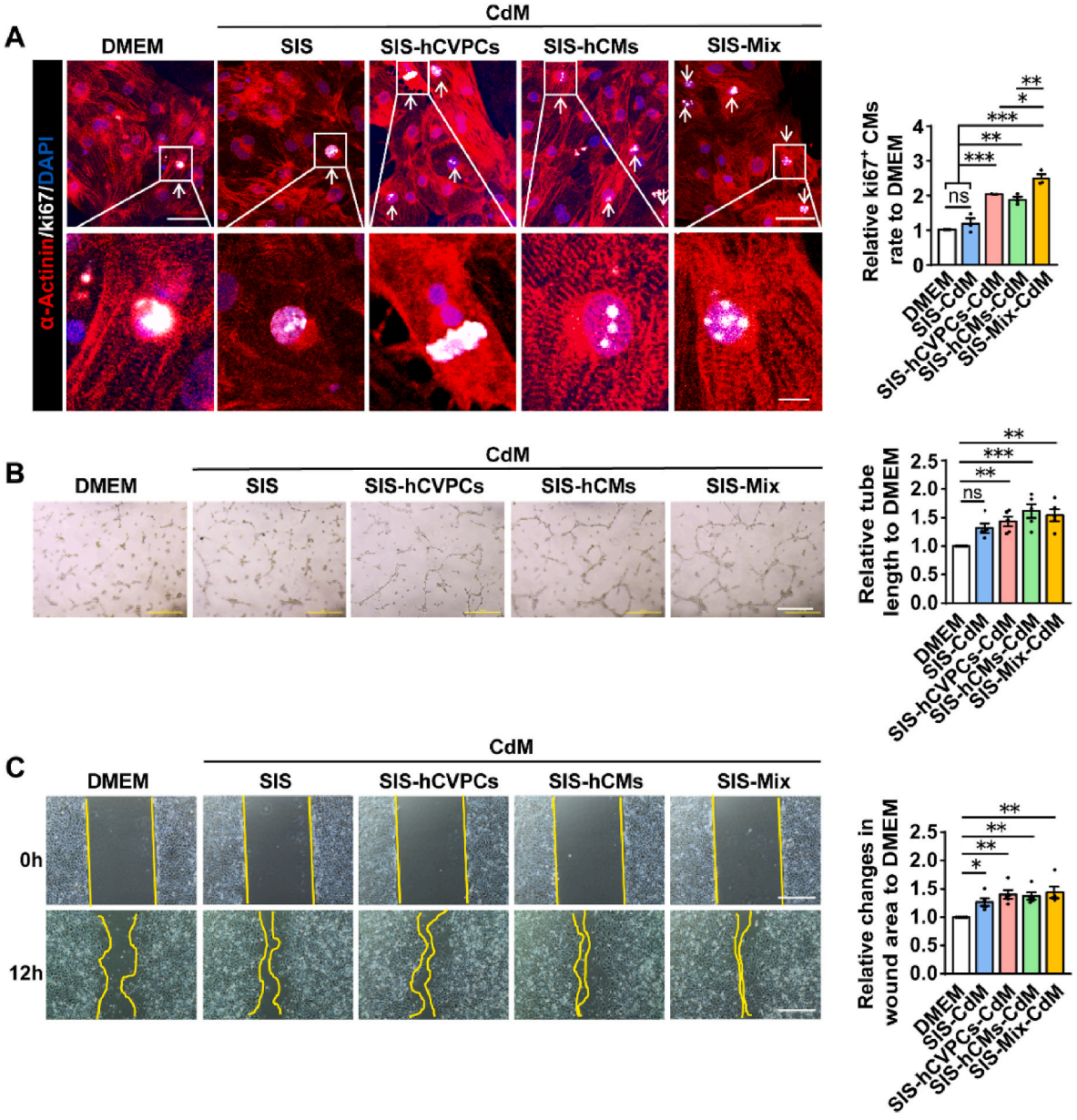

Fig. 7. The conditioned media (CdM) of cell-seeding SIS patches stimulate proliferation of cardiomyocytes (CMs) and functions of HUVECs. (A) Representative images and quantitative analysis of $ki67^{+}$ CMs co-immunocytochemical stained for ki67 and α-actinin in the hCMs incubated with various CdM for 2 days. Scale bar, 50 μm (upper panels) and 10 μm (lower panels). n = 3 independent repeats. **(B)** Representative images and quantitative analysis of tube formation of HUVECs incubated with various CdM for 24 h. Scale bar, 500 μm. n = 5 independent repeats. **(C)** Views of the scratch induced in the HUVEC monolayer and wound invasion after incubation for 12 h with various CdM. Scale bar, 500 μm. All values were mean ± SEM. $^{*}p < 0.05$, $^{**}p < 0.01$, $^{***}p < 0.001$; ns, no statistical significance.

mainly annotated to biological functions including cell-cell adhesion, cell migration, protein phosphorylation, signal transduction, and immune response (Fig. S13A), while these in the hCM-CdM were mainly annotated to muscle filament sliding, ATPase activity, muscle contraction, collagen fibril organization, gluconeogenesis, and skeletal system development (Fig. S13B). GOBP analysis of the proteins exclusively

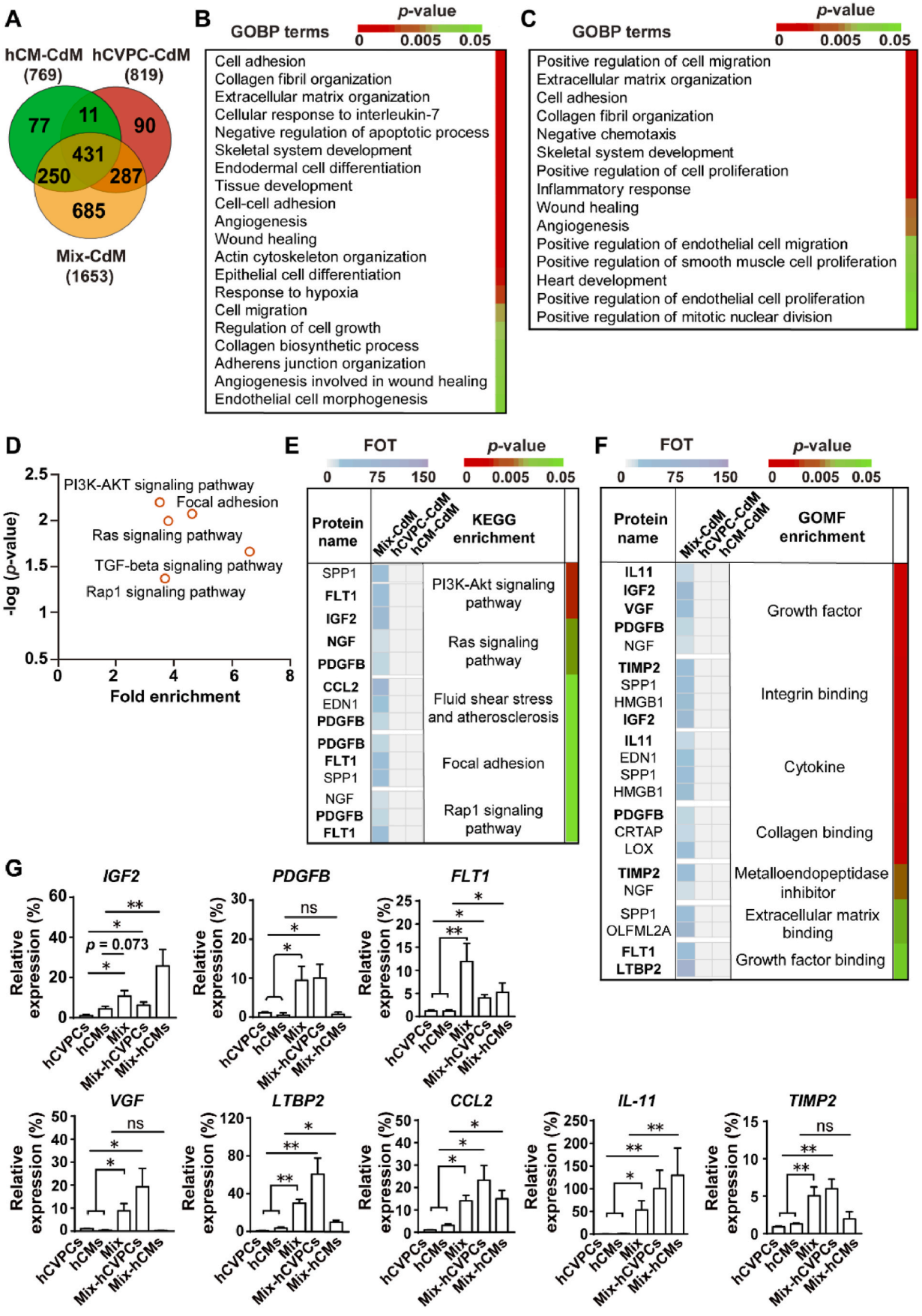

(caption on next page)

Fig. 8. Proteomic analysis of the secretome and transcript **levels in the conditioned media (CdM) of hCVPCs and hCMs with or without co-cultivation**. (**A**) Venn diagram described exclusive (identified only in one group) and shared (identified in more than one group) proteins identified in the CdM from hCVPCs, hCMs, and Mix. **(B)** Enrichment analysis of biological processes annotated by shared proteins identified in three groups subjected to gene ontology biological processes (GOBP) terms. (**C-D**) Proteins exclusively identified in the Mix-CdM were annotated for GOBP and KEGG pathway analyses. The enriched GOBP terms indicated biological processes and the associated *p*-value for the statistical confidence (**C**). Statistically enriched pathways identified by KEGG analysis (**D**). (**E-F**) The proteins with high expression in the Mix-CdM were classified to reported molecular functions (**E**) and involved pathways (**F**) through Gene Ontology Molecular Function (GOMF) and KEGG analyses. Representative molecular function and pathways (p-value <0.05) were showed. The horizontal bar graph (left side) specifies the abundance of each protein in the hCVPC-CdM, hCM-CdM, and Mix-CdM. The colors of vertical bar graph (right side) mark the *p*-value. **(G)** RT-qPCR analysis of the expression of genes coding the proteins with high abundance and involvement of functions or pathways (highlighted in Fig. 8E and F and more detailed in Tables S4–S5) in the hCVPCs, hCMs, Mix and FACS-sorted hCVPCs or hCMs from Mix (Mix-hCVPCs, Mix-hCMs). All values were expressed as mean ± SEM. n = 5–6 for each group. Unpaired *t*-test was used for statistical analyses. $*p < 0.05$, $**p < 0.01$; ns: no statistical significance.

detected in the Mix-CdM showed that they were significantly enriched in positive regulations of cell migration, cell adhesion, collagen organization, cell proliferation, inflammation, wound healing, and angiogenesis (Fig. 8C). Moreover, GO cellular compartmentalization analysis showed that about 32.7% of secreted proteins were annotated to the exosomal cargo in the Mix-CdM (Table S2), suggesting an alteration of exosomal secretion profile by the interaction of hCVPCs and hCMs. Further analysis of the pathway enrichment in Kyoto Encyclopedia of Genes and Genomes (KEGG) terms revealed that the secretome was significantly enriched in PI3K-AKT, Ras, TGF-beta, and Rap1 signaling pathways (Fig. 8D). Consistently, the enrichment analyses of KEGG pathway and molecule functions for proteins exclusively detected in the Mix-CdM with high expression (presented in the list of Table S3) further showed that the secretome was enriched in PI3K-AKT, Ras, TGF-beta, and Rap1 signaling pathways (Fig. 8E, Table S4) and actively involved in growth factor, growth factor binding, ECM binding, and cytokines (Fig. 8F, Table S5). The expression of genes coding the proteins (highlighted in Fig. 8E and F), which involved in molecular functions or pathways as shown in Tables S3–S4, was further verified by RT-qPCR analysis (Fig. 8G). Supportively, the transcript levels of the genes including *PDGFB*, *FLT1*, *VGF*, LTBP2, *CCL2*, *IL-11*, and *TIMP2* were higher in co-cultivated hCVPCs and hCMs than these in mono-cells, while the transcript level of *IGF2* did not achieve significant differences between the hCMs and the Mix (Fig. 8G). Interestingly, most of them, such as *IGF2*, *FLT1*, *TLBP2*, *CCL2*, and *IL-11*, were up-regulated in both hCVPCs and hCMs after co-cultivation, while the *PDGFB*, *VGF*, and *TIMP2* were only up-regulated in the hCVPCs sorted from the Mix (Fig. 8G). These results indicate the variable plasticity following the intercellular interaction between hCVPCs and hCMs and diversified paracrine ability of hCVPCs and hCMs.

4. Discussion

This study reported the compatibility of ECM patches with the mono- and dual-hCVPCs + hCMs and side-by-side compared their efficacy for the treatment of subacute MI in a rodent model. The results showed that (i) the SIS-ECM has good biocompatibility to hCVPCs and hCMs; (ii) epicardial implantation of SIS-hCVPC, SIS-hCM, and SIS-Mix patches at day 7 post-MI significantly preserves cardiac function and decreases scar formation at day 28 post-implantation but not the SIS alone, concomitantly associated with increased vascularization and cardiomyocyte proliferation; (iii) implantation of the SIS-Mix patches has better therapeutic effects characterized by more effective short- and long-term improvements of LV performance and dilation, and enhancement of cardiomyocyte proliferation and engraftment; and (iv) the detected proteins in the hCVPC-CdM and hCM-CdM are involved in unique functional processes essential for repair, and co-culture of hCVPCs and hCMs stimulates the secretome with more unique paracrine factors related to growth factors, cytokines, ECM organization, and cell proliferation, as well as activation of PI3K-Akt, TGF-beta, Ras, and Rap1 signaling pathways. These findings extend previous findings and provide new approaches to strengthen therapeutic benefits of hCVPCs and hCMs in the treatment of infarcted hearts. The new knowledge involved in paracrine responses to the intercellular interaction between hCVPCs and hCMs would help to promote the identification of valuable paracrine factors and the development of potential non-cell therapeutic approaches to facilitate infarct healing.

One of major findings in this study is the good support to the growth of hPSC-derived cardiac lineage cells by the SIS patches. Although combinations of cells with the ECM have been widely studied for cardiac repair and regeneration [14,18,52,53] and the SIS-ECM supports the growth of seeded human and porcine MSCs [21,29] and mCPCs [28], our study extended the seeding cell types by demonstrating the increased cell viability of hCVPCs, hCMs, and mixture on the SIS compared with the cell culture alone. Moreover, the hCVPCs and hCMs had compact adhesion with the SIS and maintained the expression of their markers and synchronous contraction in the hCM seeding-SIS patch. Furthermore, consistent with previous studies showing the recruitment of host cells to the SIS scaffold and completely absorbed by 90 days *in vivo* [54,55], this study showed integration of the SIS with the host myocardium at 90 days post-implantation (Fig. S11B) and recruitment of host cells to the SIS patches as well as formed vessels in the infarcted hearts (Fig. 5C and D; Fig. 6D). This effect seems mainly caused by the paracrine communication between the SIS-ECM and the host vessel cells as the promotion of endothelial cell migration by the SIS-CdM (Fig. 7C). Thus, the collagen-rich SIS-ECM not only has good compatibility with hPSC-derived cardiac lineage cells, but also interacts with the host cells to form vessels to support seeded and host cells for cardiac repair.

Secondly, this study compared therapeutic effects side-by-side among SIS patches, hCVPC-, hCM-, and hCVPC + hCM-SIS patches for infarcted hearts. Epicardial implantation of hCVPC-, hCM-, and their Mix-seeding SIS patches at day 7 post-infarction significantly preserved the heart function and reduced scar formation at 28 and 90 days post-implantation, concomitantly with promoted cardiomyocyte proliferation, vascularization, and remuscularization as well as decreased LV remodeling (Figs. 2–6; Fig. S7–S9). These beneficial effects were greater than the SIS patch alone. The improvements of SIS patch in cardiac function and angiogenesis observed here are consistent with a previous study with the epicardially implanted SIS-ECM at acute phase of a rat MI model [19]. Moreover, the improvement of cardiac function by the SIS-ECM in our study was only observed at 90 days but not 28 days post-implantation and the MI-caused LV dilation and scar formation remained unchanged at both 28 and 90 days post-implantation. Similar non-significant effects of the SIS-ECM in the cardiac function and dilation as well as scar size were observed at 28 days post-implantation in nude mice [28]. It seems that the SIS patch-promoted capillary and arterial vessel formation may contribute to the long-term improvement of cardiac function, while it is not enough to significantly improve cardiac function and LV dilation in early days and prevent the progress of fibrosis formation. In addition, differed from the previous report showing that the SIS-ECM alone did not reduce the mRNA expression of *Anp*, *Bnp*, *Col1*, and *Col3* in the infarcted heart of nude mice [28], we found the expression of these gene was inhibited by the SIS patches in the infarcted hearts. This may be due to the different mouse models (nude mice vs. the mice with the immunosuppressant) and the implantation time (immediately following MI vs. 7 days post-MI).

Stimulation of cardiomyocyte proliferation in the infarcted hearts is

important for repair of infarcted hearts. Epicardial implantation of human cardiac muscle patches made from hiPSC-derived smooth muscle cells, ECs and hCMs with fibrin scaffold has been shown to promote cardiomyocyte proliferation in a porcine model of MI [14] and endothelialized patches with fibrin gel spiked with human CSCs were also proved to enhance cardiomyocyte proliferation in a rat MI model [56]. Our data further demonstrated that cardiomyocyte proliferation in the border zone of infarcted hearts could be stimulated by mono-hCVPC- and hCM- or their Mix-seeding SIS patches. This is mediated by the paracrine action of seeded cells as the cardiomyocyte proliferation remained unchanged in the SIS patch-treated infarcted hearts and the enhanced number of $Ki67^+$ cardiomyocytes was only observed in the CdM from these cells but not the CdM of SIS patch. Supportively, cardiomyocyte proliferation stimulated by hPSC-derived cardiac lineage cells was reported to be mediated by secreted exosomes [14]. Another challenge for cell therapy is low retention of implanted cells. Although injection of hCVPCs could promote infarcted heart repair, these studies failed to detect significant grafts of vessels or cardiomyocytes derived from hCVPCs in both rodent and nonhuman primate models of MI [4,12]. Because the improvement of infarcted heart function is correlated with the engraftment of hPSC-derived cardiomyocytes [57–59], enhancement of cell retention is a way to increase the efficiency of cardiac repair. Our data showed the better cell retention of the SIS-cell patches than the cell injection (Fig. S5). Moreover, in the SIS-hCVPC- and SIS-Mix-treated groups, simultaneous co-expression of GFP^+ engrafted cells with cardiomyocyte and vascular cell markers were observed in the infarcted hearts (Fig. 6D) and co-expression of GFP^+ engrafted cells with the vascular cell marker were detected in the grafted patches (Fig. 5D). These results suggest the intrinsic differentiation capacity of hCVPCs into cardiovascular cells *in vivo* and their roles in the promoting of cardiac repair need to be further improved.

Thirdly, our study uncovered therapeutic similarities and differences among SIS-hCVPC, SIS-hCM, and SIS-Mix groups after epicardial delivery to subacute MI hearts in a rodent model. Consistent with the previous study showing similar improvements of cardiac function, dilation and reduction of scar size at 28 days after intramyocardial injection of hCVPCs and hCMs in a nude rat ischemia/reperfusion (I/R) model [11], the comparable improvements in LV functional and dilation as well as the reduction of scar formation were observed in both SIS-hCVPC- and SIS-hCM-treated infarcted hearts at 28 days and 90 days post-implantation. These effects were accompanied by similar improvements of cardiomyocyte hypertrophy and increases of cardiomyocyte proliferation as well as vascularization. However, hCVPCs and hCMs showed comparable low retention in the intramyocardial injected I/R hearts [11], while the SIS-hCVPC patches showed prolonged grafts (Fig. 6C). The difference may be caused by different rodent models (nude rat model vs. immunosuppressive mice), severity of MI (I/R vs. permanent MI), implanted cell doses (10×10^6 cells vs. 2×10^5 cells) and implantation ways (intramyocardial injection vs. epicardial implantation). Furthermore, the SIS-hCM and SIS-Mix but not SIS-hCVPC patches significantly increased the ratio of collagen III/I fibers in infarcted hearts, though all of the cell-seeding patches reduced the transcript levels of *Col1* and *Col3* in the infarct myocardium (Fig. S8). Supportively, the unique proteins detected in the hCM-CdM and Mix-CdM were enriched in collagen organization (Fig. 8C and Fig. S13B). The ratio of collagen subtypes is proposed to regulate compliance in remodeling myocardium and the high level of collagen I might increase myocardial stiffness because it forms thicker and stiffer fibers, whereas the collagen III fibers are more compliant and elastic [60,61]. Thus, the paracrine effects of the SIS-hCMs and SIS-Mix might contribute to the modulation of stiffness of fibrotic infarct area via regulating collagen fibers, and subsequently contribute to the improvement of the wall motion. This possibility needs to be further verified.

Interestingly, SIS-Mix patches showed significantly improvements of LV function and chamber dilation at both 28 and 90 days post-implantation, accompanied with better promotion of cardiomyocyte proliferation and cells retention than mono-cell ones. Cell therapy of hCMs combining with MSCs, epicardial cells, or ECs, and smooth muscle cells was reported for promotion of infarcted healing [14,62–65], whereas our study revealed previously unrecognized synergistic effects of dual hCVPC- and hCM-seeded SIS patches in cardiac repair. The enhanced outcomes seem unlikely related to the improved angiogenesis as the increased capillary density and small vessels in the infarcted hearts were similar between the dual cell patches and mono-cell patches. Instead, we demonstrated markedly enhanced generation of new cardiomyocytes characterized by more cardiomyocytes with cell cycle activity ($Ki67^+$), undergoing M-phase/mitosis ($PH3^+$) and cytokinesis (Aurora B^+) at 28 days post-implantation in the SIS-Mix group than these in the SIS-hCVPC and SIS-hCM groups. In addition, co-expression of GFP^+ $cTnT^+$ cells and GFP^+ α-SMA^+ vessels were detected in SIS-hCVPC- and SIS-Mix-treated infarcted hearts but not in the SIS-hCM-treated one at 90 days post-implantation. Notably, the hCVPC-derived vasculogenesis participated in the increased vascularity observed in the SIS-hCVPC and SIS-Mix patches (Fig. 5C–D) and the arterioles in these engrafted patches seemed connected with these in the host myocardium (Fig. 5E). These observations suggest survival of implanted cells and differentiation of hCVPCs to cardiovascular cells, which is supposed to improve the challenging infarct environment and grafts survival after epicardial implantation [44]. Supportively, the CVPCs were observed to self-organize into the vascular system in the infarct hearts through differentiation [66]. Moreover, as the extracellular vesicles and cellular factors secreted from hCVPCs are demonstrated to improve the survival of cardiomyocytes and stimulate vascularization [4,12,38,67], the paracrine action of hCVPCs may play important roles in these outcomes. Considering more GFP^+ $cTnT^+$ cells and similar number of GFP^+ α-SMA^+ vessels were observed in the SIS-Mix-treated myocardium compared with these in the mono cell-seeding SIS-treated groups at 90 days post-implantation even though the former was only half number of each cell type compared with the latter, the interaction of hCVPCs and hCMs might stimulate more paracrine factors favoriting maintenance of cell retention and survival as well as stimulation of cardiomyocyte formation than hCVPCs alone. This is supported by the quantitative secretome analysis of the CdM from these cell types with and without co-cultivation discussed below. Collectively, these findings reveal the values of SIS-hCVPC, SIS-hCM, and SIS-Mix patches in promoting infarct repair, while the SIS-Mix patches synergistically amplify advantages of hCVPCs and hCMs. The synergistic effect of SIS-Mix patches needs to be further strengthened by identification of the optimal ratio of hCVPCs and hCMs and the dose via examination of dose-dependency of repair efficacy *in vivo*. Considering the approvement of SIS-ECM for cardiac patching by the Food and Drug Administration [26] and the technical feasibility and safety of epicardial delivery of hCVPC [16] and hCM patches [17] in patients with severe ischemic cardiomyopathy, the hPSC-derived cardiac lineage cell-based ECM patches are promising for clinical application and need to be further investigated in large animal models. More efforts are needed to scale up cell dose and improve long-term engraftment of hCVPCs and hCMs, which are critical to compensate the lost cardiomyocytes as well as maintain efficient paracrine effects for promoting cardiac repair and regeneration.

Finally, the comparative proteomic analysis revealed secretome profiles of mono-hCVPCs, hCMs and their Mix and uncovered potential mechanisms associated with their beneficial effects. Along with the similar increases in functional improvement, LV remodeling, vascularization and cardiomyocyte proliferation *in vivo* study with the cell-seeding SIS patches as well as HUVEC migration, tube formation, and cardiomyocyte proliferation *in vitro* study, GOBP analysis showed that the overlapping proteins were enriched in biological functions, including cell adhesion, migration, anti-apoptosis, ECM organization, tissue development, wound healing, cell growth, and angiogenesis, etc. The data are consistent with the findings from hCMs [57] and the

neonatal human CPC-CdM [68]. Besides the similarity of paracrine effects shared between the hCVPCs and the hCMs, their distinct paracrine characteristics were identified in this study. Consistent with our previous observations showing the modulation of macrophage polarization by hCVPC-secreted cytokine-induced STAT6 activation [12], the unique proteins in the hCVPC-CdM annotated by GOBP terms were related to the protein phosphorylation, signal transduction, and immune response. In line with the significant modulation of collagen fibers by the SIS-hCM patches in the infarcted hearts, the unique proteins regulating collagen fibril organization were detected in the hCM-CdM. Meanwhile, the secreted proteins in the hCM-CdM were involved in the improvement of contractile force. This is supported by a recent report showing the contractile force of implanted hCMs actively involved in the mechanical function of injured heart [69] and the initial results from epicardial implantation of hiPSC-CM patches in a patient with ischemic cardiomyopathy showing recovery of the wall motion in the implanted site [17]. Further studies are needed to identify unique factors secreted from hCVPCs and hCMs for the promoting of cardiac repair and to investigate the unique paracrine effects of hCMs compared with other cell sources, such as MSCs, ECs, and fibroblasts in future.

Notably, much more unique proteins were detected in the Mix-CdM than these in the hCVPC-CdM and hCM-CdM (~41% vs. ~10%–11%). The CdM from I/R injured hCMs caused upregulation of hCPC proteins associated with migration and proliferation [70]. Here, we provided new evidence showing more new proteins secreted following the interaction of hCVCPs and hCMs. The enriched functional processes were related to vascular cells proliferation, heart development, mitotic nuclear division, and the enriched PI3K-AKT and TGF-beta signaling pathways were related the activation of cardiomyocyte proliferation and/or cell cycle progression as reported [71,72]. Therefore, the cell-cell interaction between hCVPCs and hCMs may endow them with powerful endurance to modulate ischemic environment, resulting in stronger beneficial effects in promoting infarct repair. It is noteworthy that these unique proteins with high abundance appeared to induce similar pathways involved in pro-proliferation and occupy cardioprotective properties (Fig. 8E and F, Tables S3 and S4). In fact, the mRNA levels of IGF2 and PDGFB were significantly elevated in the co-cultivated hCMs or hCVPCs (Fig. 8G), which may contribute to the synergetic paracrine effects of the SIS-Mix patches in the improvement of cell retention and proliferative cardiomyocytes. This is supported by the observations of promoted LV function and proliferative cells in the hearts treated with IGF-2-overexpressing endothelial progenitor cells [73] and improved cardiomyocyte survival through implanted hCM-secreted PDGF-BB [74]. Similarly, the transcripts of IL11, CCL2, and TIMP2 (crucial determinants of fibrosis [75], inflammation [76], and remodeling [77] after MI) were all up-regulated after co-culture. These changes might contribute to the SIS-Mix patch-mediated repairing of infarcted hearts since the IL11 has been reported to protect hearts from prolonged hypothermic ischemia [78] and TIMP2-overexpressing MSC-derived exosome showed enhanced repair effect in rat MI model [79]. Interestingly, the transcript of FLT1, suggested to exclusively express in ECs [80] was upregulated after cell co-culture of hCVPCs and hCMs (Fig. 8G). Therefore, the paracrine effects seem play important roles in the outcomes of SIS-hCVPC, SIS-hCM, and SIS-Mix patches in the infarcted hearts. Supportively, the CdM from SIS-hCVPCs, SIS-hCMs, and SIS-Mix all promoted tube formation and wound healing ability of ECs, as well as enhanced the cardiomyocyte proliferation (Fig. 7). Moreover, the CdM from SIS-Mix stimulated cardiomyocyte proliferation stronger than that from the mono-cell seeding SIS as observed in the *in vivo* study (Figs. 4 and 7A). Furthermore, the interaction of hCVPCs and hCMs seemed change their exosomal secretion profile (Table S2). These findings provide an integrated picture of the modulated secretomes and activated state of key signaling pathways following hCVPCs and hCMs interaction. Whether the candidate paracrine factors and altered exosomal cargo by the interaction of hCVPCs and hCMs contributes to the better effects in promoting of cardiac repair needs to be verified in future.

4.1. Limitations

The findings we obtained here are based on a murine model of MI. Following important issues for the cardiac patches need to be further investigated in large animal models of MI: (i) whether the beating cardiac patches could synchronize with the wall motion in the implanted site; (ii) whether the cardiac patches could improve the stiffness of fibrotic infarct area; and (iii) whether the cardiac patch can electrically integrate or cause the incidence of arrhythmia in the recipient's hearts.

5. Conclusion

We develop a strategy for promoting cardiac repair with engineered mono- and dual-hCVPC and hCM-seeding SIS patches, which displays long-term functional improvements, smaller scar and reversed maladaptive remodeling in the infarcted hearts when epicardially implanted at the sub-acute phase of MI. The beneficial effects are associated with enhanced cardiomyocyte proliferation, modulated collage components, promoted revascularization, and prolonged cell engraftment. The results from treatments of cardiovascular cells with the CdM from mono- and dual-hCVPCs and hCMs, combining with the proteome analysis, further suggest that the paracrine effects play important roles in the beneficial effects of cell-seeding SIS patches. Moreover, the dual cell-seeding patches show better functional improvement, cardiomyocyte proliferation and engraftment in the treated hearts. Supportively, the unique secretome involved in cardioprotective processes and enriched in pathways essential for cell proliferation and functional recovery following co-culture of hCVPCs and hCMs highlights the importance of the interaction between hCVPCs and hCMs. These results suggest that the implantation of dual hCVPC- and hCM-seeding SIS patches exhibits synergistic and complementary effects in promoting infarct repair, which might be a promising therapeutic approach for ischemic hearts disease.

Funding

This work was supported by grants from National Key R&D Program of China (2022YFA1105100 to H.-T.Y., 2017YFA 0103700, 2022YFA1104500; 2017YFA0105600 to Z.-M.L.); the Strategic Priority Research Program of the Chinese Academy of Sciences (No. XDA16010201 to H.-T.Y.), and National Natural Science Foundation of China (81520108004).

Data and materials availability

All data needed to evaluate the conclusions in the paper are present in the paper and/or the Supplementary Materials. Additional data related to this paper may be requested from the authors.

Ethics approval and consent to participate

All surgical procedures were performed in accordance with the Guidelines for Care and Use of Laboratory Animals published by the US National Institutes of Health (NIH Publication, 8th Edition, 2011) and were approved by the Institutional Animal Care and Use Committee of Shanghai Institutes of Nutrition and Health.

CRediT authorship contribution statement

Yun Jiang: Conceptualization, Methodology, Investigation, Visualization, Formal analysis, Validation, Writing – original draft. **Ling-Ling Zhang:** Methodology, Resources, Writing – original draft. **Fan Zhang:** Methodology, Investigation, Data curation, Software, Writing – original draft. **Wei Bi:** Investigation. **Peng Zhang:** Validation, Funding

acquisition. **Xiu-Jian Yu:** Methodology, Writing – original draft. **Sen-Le Rao:** Investigation. **Shi-Hui Wang:** Investigation. **Qiang Li:** Conceptualization, Project administration, Funding acquisition. **Chen Ding:** Methodology, Data curation, Software, Funding acquisition. **Yin Jin:** Methodology, Resources, Funding acquisition. **Zhong-Min Liu:** Funding acquisition. **Huang-Tian Yang:** Conceptualization, Resources, Project administration, Supervision, Writing – review & editing, Funding acquisition.

Declaration of competing interest

The authors declare no competing interests.

Acknowledgements

We thank technical supports from Jin-Xi Wang, Qiang Wu and Ji-Liang Tan in the Laboratory of Molecular Cardiology as well as Yu-Jia Zhai and Yi-Fan Bu from the co-facility of Shanghai Institute of Nutrition and Health, CAS; and Zheng Li from Shanghai General Hospital. We also thank Shanghai Baiyiyuan Bioengineering Company for providing the SIS-ECM.

Appendix A. Supplementary data

Supplementary data to this article can be found online at https://doi.org/10.1016/j.bioactmat.2023.05.015.

References

[1] S.S. Virani, A. Alonso, H.J. Aparicio, E.J. Benjamin, M.S. Bittencourt, C. W. Callaway, A.P. Carson, A.M. Chamberlain, S. Cheng, F.N. Delling, M.S.V. Elkind, K.R. Evenson, J.F. Ferguson, D.K. Gupta, S.S. Khan, B.M. Kissela, K.L. Knutson, C. D. Lee, T.T. Lewis, J. Liu, M.S. Loop, P.L. Lutsey, J. Ma, J. Mackey, S.S. Martin, D. B. Matchar, M.E. Mussolino, S.D. Navaneethan, A.M. Perak, G.A. Roth, Z. Samad, G.M. Satou, E.B. Schroeder, S.H. Shah, C.M. Shay, A. Stokes, L.B. VanWagner, N. Y. Wang, C.W. Tsao, E. American Heart Association Council on, C. Prevention Statistics, S. Stroke Statistics, Heart disease and stroke statistics-2021 update: a report from the American Heart Association, Circulation 143 (8) (2021) e254–e743, https://doi.org/10.1161/CIR.0000000000000950.

[2] X. Wu, M.R. Reboll, M. Korf-Klingebiel, K.C. Wollert, Angiogenesis after acute myocardial infarction, Cardiovasc. Res. 117 (5) (2021) 1257–1273, https://doi.org/10.1093/cvr/cvaa287.

[3] T. Eschenhagen, K. Ridders, F. Weinberger, How to repair a broken heart with pluripotent stem cell-derived cardiomyocytes, J. Mol. Cell. Cardiol. 163 (2022) 106–117, https://doi.org/10.1016/j.yjmcc.2021.10.005.

[4] K.Y. Zhu, Q. Wu, C. Ni, P. Zhang, Z.W. Zhong, Y. Wu, Y.C. Wang, Y.C. Xu, M. J. Kong, H.F. Cheng, Z.H. Tao, Q. Yang, H. Liang, Y. Jiang, Q.J. Li, J. Zhao, J. J. Huang, F.J. Zhang, Q. Chen, Y. Li, J.H. Chen, W. Zhu, H. Yu, J.Y. Zhang, H. T. Yang, X.Y. Hu, J.A. Wang, Lack of remuscularization following transplantation of human embryonic stem cell-derived cardiovascular progenitor cells in infarcted nonhuman primates, Circ. Res. 122 (7) (2018) 958–969, https://doi.org/10.1161/Circresaha.117.311578.

[5] Y.W. Liu, B. Chen, X. Yang, J.A. Fugate, F.A. Kalucki, A. Futakuchi-Tsuchida, L. Couture, K.W. Vogel, C.A. Astley, A. Baldessari, J. Ogle, C.W. Don, Z. L. Steinberg, S.P. Seslar, S.A. Tuck, H. Tsuchida, A.V. Naumova, S.K. Dupras, M. S. Lyu, J. Lee, D.W. Hailey, H. Reinecke, L. Pabon, B.H. Fryer, W.R. MacLellan, R. S. Thies, C.E. Murry, Human embryonic stem cell-derived cardiomyocytes restore function in infarcted hearts of non-human primates, Nat. Biotechnol. 36 (7) (2018) 597–605, https://doi.org/10.1038/nbt.4162.

[6] Y. Jiang, X.L. Lian, Heart regeneration with human pluripotent stem cells: prospects and challenges, Bioact. Mater. 5 (1) (2020) 74–81, https://doi.org/10.1016/j.bioactmat.2020.01.003.

[7] P. Menasche, Cell Therapy with Human ESC-derived cardiac cells: clinical perspectives, Front. Bioeng. Biotechnol. 8 (2020), 601560, https://doi.org/10.3389/fbioe.2020.601560.

[8] R. Bolli, A. Kahlon, Time to end the war on cell therapy, Eur. J. Heart Fail. 22 (5) (2020) 893–897, https://doi.org/10.1002/ejhf.1767.

[9] Y. Soma, Y. Morita, Y. Kishino, H. Kanazawa, K. Fukuda, S. Tohyama, The present state and future perspectives of cardiac regenerative therapy using human pluripotent stem cells, Front Cardiovasc Med 8 (2021), 774389, https://doi.org/10.3389/fcvm.2021.774389.

[10] Y. Shiba, T. Gomibuchi, T. Seto, Y. Wada, H. Ichimura, Y. Tanaka, T. Ogasawara, K. Okada, N. Shiba, K. Sakamoto, D. Ido, T. Shiina, M. Ohkura, J. Nakai, N. Uno, Y. Kazuki, M. Oshimura, I. Minami, U. Ikeda, Allogeneic transplantation of iPS cell-derived cardiomyocytes regenerates primate hearts, Nature 538 (7625) (2016) 388–391, https://doi.org/10.1038/nature19815.

[11] S. Fernandes, J.J.H. Chong, S.L. Paige, M. Iwata, B. Torok-Storb, G. Keller, H. Reinecke, C.E. Murry, Comparison of human embryonic stem cell-derived cardiomyocytes, cardiovascular progenitors, and bone marrow mononuclear cells for cardiac repair, Stem Cell Rep. 5 (5) (2015) 753–762, https://doi.org/10.1016/j.stemcr.2015.09.011.

[12] J. Wang, M. Liu, Q. Wu, Q. Li, L. Gao, Y. Jiang, B. Deng, W. Huang, W. Bi, Z. Chen, Y.E. Chin, C. Paul, Y. Wang, H.T. Yang, Human embryonic stem cell-derived cardiovascular progenitors repair infarcted hearts through modulation of macrophages via activation of signal transducer and activator of transcription 6, Antioxidants Redox Signal. 31 (5) (2019) 369–386, https://doi.org/10.1089/ars.2018.7688.

[13] Q. Li, J. Wang, Q. Wu, N. Cao, H.T. Yang, Perspective on human pluripotent stem cell-derived cardiomyocytes in heart disease modeling and repair, Stem Cells Transl Med 9 (10) (2020) 1121–1128, https://doi.org/10.1002/sctm.19-0340.

[14] L. Gao, Z.R. Gregorich, W. Zhu, S. Mattapally, Y. Oduk, X. Lou, R. Kannappan, A. V. Borovjagin, G.P. Walcott, A.E. Pollard, V.G. Fast, X. Hu, S.G. Lloyd, Y. Ge, J. Zhang, Large cardiac muscle patches engineered from human induced-pluripotent stem cell-derived cardiac cells improve recovery from myocardial infarction in swine, Circulation 137 (16) (2018) 1712–1730, https://doi.org/10.1161/CIRCULATIONAHA.117.030785.

[15] R. Romagnuolo, H. Masoudpour, A. Porta-Sanchez, B. Qiang, J. Barry, A. Laskary, X. Qi, S. Masse, K. Magtibay, H. Kawajiri, J. Wu, T. Valdman Sadikov, J. Rothberg, K.M. Panchalingam, E. Titus, R.K. Li, P.W. Zandstra, G.A. Wright, K. Nanthakumar, N.R. Ghugre, G. Keller, M.A. Laflamme, Human embryonic stem cell-derived cardiomyocytes regenerate the infarcted pig heart but induce ventricular tachyarrhythmias, Stem Cell Rep. 12 (5) (2019) 967–981, https://doi.org/10.1016/j.stemcr.2019.04.005.

[16] P. Menasche, V. Vanneaux, A. Hagege, A. Bel, B. Cholley, A. Parouchev, I. Cacciapuoti, R. Al-Daccak, N. Benhamouda, H. Blons, O. Agbulut, L. Tosca, J. H. Trouvin, J.R. Fabreguettes, V. Bellamy, D. Charron, E. Tartour, G. Tachdjian, M. Desnos, J. Larghero, Transplantation of human embryonic stem cell-derived cardiovascular progenitors for severe ischemic left ventricular dysfunction, J. Am. Coll. Cardiol. 71 (4) (2018) 429–438, https://doi.org/10.1016/j.jacc.2017.11.047.

[17] S. Miyagawa, S. Kainuma, T. Kawamura, K. Suzuki, Y. Ito, H. Iseoka, E. Ito, M. Takeda, M. Sasai, N. Mochizuki-Oda, T. Shimamoto, Y. Nitta, H. Dohi, T. Watabe, Y. Sakata, K. Toda, Y. Sawa, Case report: transplantation of human induced pluripotent stem cell-derived cardiomyocyte patches for ischemic cardiomyopathy, Front Cardiovasc Med 9 (2022), 950829, https://doi.org/10.3389/fcvm.2022.950829.

[18] M.Y. Tan, W. Zhi, R.Q. Wei, Y.C. Huang, K.P. Zhou, B. Tan, L. Deng, J.C. Luo, X. Q. Li, H.Q. Xie, Z.M. Yang, Repair of infarcted myocardium using mesenchymal stem cell seeded small intestinal submucosa in rabbits, Biomaterials 30 (19) (2009) 3234–3240, https://doi.org/10.1016/j.biomaterials.2009.02.013.

[19] H.E.M. Mewhort, D.A. Svystonyuk, J.D. Turnbull, G. Teng, D.D. Belke, D. G. Guzzardi, D.S. Park, S. Kang, M.D. Hollenberg, P.W.M. Fedak, Bioactive extracellular matrix scaffold promotes adaptive cardiac remodeling and repair, JACC Basic Transl Sci 2 (4) (2017) 450–464, https://doi.org/10.1016/j.jacbts.2017.05.005.

[20] A. Khanna, M. Zamani, N.F. Huang, Extracellular matrix-based biomaterials for cardiovascular tissue engineering, J Cardiovasc Dev Dis 8 (11) (2021), https://doi.org/10.3390/jcdd8110137.

[21] C.W. Chang, T. Petrie, A. Clark, X. Lin, C.S. Sondergaard, L.G. Griffiths, Mesenchymal stem cell seeding of porcine small intestinal submucosal extracellular matrix for cardiovascular applications, PLoS One 11 (4) (2016). ARTN e015341210.1371/journal.pone.0153412.

[22] D. Bejleri, M.E. Davis, Decellularized extracellular matrix materials for cardiac repair and regeneration, Adv Healthc Mater 8 (5) (2019), e1801217, https://doi.org/10.1002/adhm.201801217.

[23] V. Vasanthan, H.B. Shim, G. Teng, D. Belke, D. Svystonyuk, J.F. Deniset, P.W. M. Fedak, Acellular biomaterial modulates myocardial inflammation and promotes endogenous mechanisms of postinfarct cardiac repair, J. Thorac. Cardiovasc. Surg. (2021), https://doi.org/10.1016/j.jtcvs.2021.12.036.

[24] C.M. Ramos, J.C. Francisco, M. Olandoski, K.A. Carvalho, R. Cunha, B.O. Erbano, L. F. Jorge, C.P. Baena, V.F. Amaral, L. Noronha, R.M. Macedo, J.R. Faria-Neto, L. C. Guarita-Souza, Myocardial regeneration after implantation of porcine small intestinal submucosa in the left ventricle, Rev. Bras. Cir. Cardiovasc. 29 (2) (2014) 202–213, https://doi.org/10.5935/1678-9741.20140070.

[25] H.E. Mewhort, J.D. Turnbull, A. Satriano, K. Chow, J.A. Flewitt, A.C. Andrei, D. G. Guzzardi, D.A. Svystonyuk, J.A. White, P.W. Fedak, Epicardial infarct repair with bioinductive extracellular matrix promotes vasculogenesis and myocardial recovery, J. Heart Lung Transplant. 35 (5) (2016) 661–670, https://doi.org/10.1016/j.healun.2016.01.012.

[26] R.G. Witt, G. Raff, J. Van Gundy, M. Rodgers-Ohlau, M.S. Si, Short-term experience of porcine small intestinal submucosa patches in paediatric cardiovascular surgery, Eur. J. Cardio. Thorac. Surg. 44 (1) (2013) 72–76, https://doi.org/10.1093/ejcts/ezs638.

[27] F.N. Slachman, Constructive remodeling of CorMatrix extracellular matrix after aortic root repair in a 90-year-old woman, Ann. Thorac. Surg. 97 (5) (2014) e129–e131, https://doi.org/10.1016/j.athoracsur.2013.10.103.

[28] L. Wang, E.M. Meier, S. Tian, I. Lei, L. Liu, S. Xian, M.T. Lam, Z. Wang, Transplantation of Isl1(+) cardiac progenitor cells in small intestinal submucosa improves infarcted heart function, Stem Cell Res. Ther. 8 (1) (2017) 230, https://doi.org/10.1186/s13287-017-0675-2.

[29] C. Hodonsky, L. Mundada, S.Y. Wang, R. Witt, G. Raff, S. Kaushal, M.S. Si, Effects of scaffold material used in cardiovascular surgery on mesenchymal stem cells and

cardiac progenitor cells, Ann. Thorac. Surg. 99 (2) (2015) 605–611, https://doi.org/10.1016/j.athoracsur.2014.08.071.
[30] T. Li, H. Zhao, X. Han, J. Yao, L. Zhang, Y. Guo, Z. Shao, Y. Jin, D. Lai, The spontaneous differentiation and chromosome loss in iPSCs of human trisomy 18 syndrome, Cell Death Dis. 8 (10) (2017) e3149, https://doi.org/10.1038/cddis.2017.565.
[31] C. Kime, M.A. Mandegar, D. Srivastava, S. Yamanaka, B.R. Conklin, T.A. Rand, Efficient CRISPR/Cas9-based genome engineering in human pluripotent stem cells, Curr Protoc Hum Genet 88 (2016), https://doi.org/10.1002/0471142905.hg2104s88. Unit 21 4.
[32] N. Cao, H. Liang, J.J. Huang, J. Wang, Y.X. Chen, Z.Y. Chen, H.T. Yang, Highly efficient induction and long-term maintenance of multipotent cardiovascular progenitors from human pluripotent stem cells under defined conditions, Cell Res. 23 (9) (2013) 1119–1132, https://doi.org/10.1038/cr.2013.102.
[33] N. Cao, H. Liang, H.T. Yang, Generation, expansion, and differentiation of cardiovascular progenitor cells from human pluripotent stem cells, Methods Mol. Biol. 1212 (2015) 113–125, https://doi.org/10.1007/7651_2014_119.
[34] S. Bhattacharya, P.W. Burridge, E.M. Kropp, S.L. Chuppa, W.M. Kwok, J.C. Wu, K. R. Boheler, R.L. Gundry, High efficiency differentiation of human pluripotent stem cells to cardiomyocytes and characterization by flow cytometry, J. Vis. Exp. 91 (2014), 52010, https://doi.org/10.3791/52010.
[35] S. Tohyama, F. Hattori, M. Sano, T. Hishiki, Y. Nagahata, T. Matsuura, H. Hashimoto, T. Suzuki, H. Yamashita, Y. Satoh, T. Egashira, T. Seki, N. Muraoka, H. Yamakawa, Y. Ohgino, T. Tanaka, M. Yoichi, S. Yuasa, M. Murata, M. Suematsu, K. Fukuda, Distinct metabolic flow enables large-scale purification of mouse and human pluripotent stem cell-derived cardiomyocytes, Cell Stem Cell 12 (1) (2013) 127–137, https://doi.org/10.1016/j.stem.2012.09.013.
[36] H.J. Bai, P. Zhang, L. Ma, H. Liang, G. Wei, H.T. Yang, SMYD2 drives mesendodermal differentiation of human embryonic stem cells through mediating the transcriptional activation of key mesendodermal genes, Stem Cell. 38 (7) (2020) E1–E2, https://doi.org/10.1002/stem.3176.
[37] X.L. Luo, P. Zhang, X. Liu, S. Huang, S.L. Rao, Q. Ding, H.T. Yang, Myosin light chain 2 marks differentiating ventricular cardiomyocytes derived from human embryonic stem cells, Pflügers Archiv 473 (7) (2021) 991–1007, https://doi.org/10.1007/s00424-021-02578-3.
[38] W. Bi, J. Wang, Y. Jiang, Q. Li, S. Wang, M. Liu, Q. Liu, F. Li, C. Paul, Y. Wang, H. T. Yang, Neurotrophin-3 contributes to benefits of human embryonic stem cell-derived cardiovascular progenitor cells against reperfused myocardial infarction, Stem Cells Transl Med 10 (5) (2021) 756–772, https://doi.org/10.1002/sctm.20-0456.
[39] M. Xing, Y. Jiang, W. Bi, L. Gao, Y.L. Zhou, S.L. Rao, L.L. Ma, Z.W. Zhang, H. T. Yang, J. Chang, Strontium ions protect hearts against myocardial ischemia/reperfusion injury, Sci. Adv. 7 (3) (2021), eabe0726, https://doi.org/10.1126/sciadv.abe0726.
[40] Q. Wu, J. Wang, W.L.W. Tan, Y. Jiang, S. Wang, Q. Li, X. Yu, J. Tan, S. Liu, P. Zhang, Z. Tiang, Z. Chen, R.S. Foo, H.T. Yang, Extracellular vesicles from human embryonic stem cell-derived cardiovascular progenitor cells promote cardiac infarct healing through reducing cardiomyocyte death and promoting angiogenesis, Cell Death Dis. 11 (5) (2020) 354, https://doi.org/10.1038/s41419-020-2508-y.
[41] A. Kalnins, M.N. Thomas, M. Andrassy, S. Muller, A. Wagner, S. Pratschke, M. Rentsch, S. Klussmann, T. Kauke, M.K. Angele, A.V. Bazhin, M. Fischereder, J. Werner, M. Guba, J. Andrassy, Spiegelmer inhibition of MCP-1/CCR2–potential as an adjunct immunosuppressive therapy in transplantation, Scand. J. Immunol. 82 (2) (2015) 102–109, https://doi.org/10.1111/sji.12310.
[42] X. Sun, J. Wu, B. Qiang, R. Romagnuolo, M. Gagliardi, G. Keller, M.A. Laflamme, R. K. Li, S.S. Nunes, Transplanted microvessels improve pluripotent stem cell-derived cardiomyocyte engraftment and cardiac function after infarction in rats, Sci. Transl. Med. 12 (562) (2020), eaax2992, https://doi.org/10.1126/scitranslmed.aax2992.
[43] P. Kong, A.V. Shinde, Y. Su, I. Russo, B. Chen, A. Saxena, S.J. Conway, J.M. Graff, N.G. Frangogiannis, Opposing actions of fibroblast and cardiomyocyte smad3 signaling in the infarcted myocardium, Circulation 137 (7) (2018) 707–724, https://doi.org/10.1161/Circulationaha.117.029622.
[44] S.B. Riemenschneider, D.J. Mattia, J.S. Wendel, J.A. Schaefer, L. Ye, P.A. Guzman, R.T. Tranquillo, Inosculation and perfusion of pre-vascularized tissue patches containing aligned human microvessels after myocardial infarction, Biomaterials 97 (2016) 51–61, https://doi.org/10.1016/j.biomaterials.2016.04.031.
[45] S. Nuernberger, N. Cyran, C. Albrecht, H. Redl, V. Vecsei, S. Marlovits, The influence of scaffold architecture on chondrocyte distribution and behavior in matrix-associated chondrocyte transplantation grafts, Biomaterials 32 (4) (2011) 1032–1040, https://doi.org/10.1016/j.biomaterials.2010.08.100.
[46] D.N. Perkins, D.J. Pappin, D.M. Creasy, J.S. Cottrell, Probability-based protein identification by searching sequence databases using mass spectrometry data, Electrophoresis 20 (18) (1999) 3551–3567, https://doi.org/10.1002/(SICI)1522-2683(19991201)20:18.
[47] F. Zhang, Q. Zhang, J. Zhu, B. Yao, C. Ma, N. Qiao, S. He, Z. Ye, Y. Wang, R. Han, J. Feng, Y. Wang, Z. Qin, Z. Ma, K. Li, Y. Zhang, S. Tian, Z. Chen, S. Tan, Y. Wu, P. Ran, Y. Wang, C. Ding, Y. Zhao, Integrated proteogenomic characterization across major histological types of pituitary neuroendocrine tumors, Cell Res. 32 (12) (2022) 1047–1067, https://doi.org/10.1038/s41422-022-00736-5.
[48] E.N. Poon, X.L. Luo, S.E. Webb, B. Yan, R. Zhao, S.C.M. Wu, Y. Yang, P. Zhang, H. Bai, J. Shao, C.M. Chan, G.C. Chan, S.Y. Tsang, R.L. Gundry, H.T. Yang, K. R. Boheler, The cell surface marker CD36 selectively identifies matured, mitochondria-rich hPSC-cardiomyocytes, Cell Res. 30 (7) (2020) 626–629, https://doi.org/10.1038/s41422-020-0292-y.
[49] J.L. Berry, W. Zhu, Y.L. Tang, P. Krishnamurthy, Y. Ge, J.P. Cooke, Y. Chen, D. J. Garry, H.T. Yang, N.S. Rajasekaran, W.J. Koch, S. Li, K. Domae, G. Qin, K. Cheng, T.J. Kamp, L. Ye, S. Hu, B.M. Ogle, J.M. Rogers, E.D. Abel, M.E. Davis, S.D. Prabhu, R. Liao, W.T. Pu, Y. Wang, P. Ping, N. Bursac, G. Vunjak-Novakovic, J.C. Wu, R. Bolli, P. Menasche, J. Zhang, Convergences of life sciences and engineering in understanding and treating Heart Failure, Circ. Res. 124 (1) (2019) 161–169, https://doi.org/10.1161/CIRCRESAHA.118.314216.
[50] J. Zhang, R. Bolli, D.J. Garry, E. Marban, P. Menasche, W.H. Zimmermann, T. J. Kamp, J.C. Wu, V.J. Dzau, Basic and translational research in cardiac repair and regeneration: JACC state-of-the-art review, J. Am. Coll. Cardiol. 78 (21) (2021) 2092–2105, https://doi.org/10.1016/j.jacc.2021.09.019.
[51] J. Fang, J.J. Li, X. Zhong, Y. Zhou, R.J. Lee, K. Cheng, S. Li, Engineering stem cell therapeutics for cardiac repair, J. Mol. Cell. Cardiol. 171 (2022) 56–68, https://doi.org/10.1016/j.yjmcc.2022.06.013.
[52] E. Querdel, M. Reinsch, L. Castro, D. Kose, A. Bahr, S. Reich, B. Geertz, B. Ulmer, M. Schulze, M.D. Lemoine, T. Krause, M. Lemme, J. Sani, A. Shibamiya, T. Studemann, M. Kohne, C.V. Bibra, N. Hornaschewitz, S. Pecha, Y. Nejahsie, I. Mannhardt, T. Christ, H. Reichenspurner, A. Hansen, N. Klymiuk, M. Krane, C. Kupatt, T. Eschenhagen, F. Weinberger, Human engineered heart tissue patches remuscularize the injured heart in a dose-dependent manner, Circulation 143 (20) (2021) 1991–2006, https://doi.org/10.1161/CIRCULATIONAHA.120.047904.
[53] X. Zhang, X. Chen, H. Hong, R. Hu, J. Liu, C. Liu, Decellularized extracellular matrix scaffolds: recent trends and emerging strategies in tissue engineering, Bioact. Mater. 10 (2022) 15–31, https://doi.org/10.1016/j.bioactmat.2021.09.014.
[54] Z.Q. Zhao, J.D. Puskas, D. Xu, N.P. Wang, M. Mosunjac, R.A. Guyton, J. Vinten-Johansen, R. Matheny, Improvement in cardiac function with small intestine extracellular matrix is associated with recruitment of c-kit cells, myofibroblasts, and macrophages after myocardial infarction, J. Am. Coll. Cardiol. 55 (12) (2010) 1250–1261, https://doi.org/10.1016/j.jacc.2009.10.049.
[55] T.W. Gilbert, A.M. Stewart-Akers, A. Simmons-Byrd, S.F. Badylak, Degradation and remodeling of small intestinal submucosa in canine Achilles tendon repair, J. Bone Jt. Surg. Am. 89 (3) (2007) 621–630, https://doi.org/10.2106/JBJS.E.00742.
[56] T. Su, K. Huang, M.A. Daniele, M.T. Hensley, A.T. Young, J. Tang, T.A. Allen, A. C. Vandergriff, P.D. Erb, F.S. Ligler, K. Cheng, Cardiac stem cell patch integrated with microengineered blood vessels promotes cardiomyocyte proliferation and neovascularization after acute myocardial infarction, ACS Appl. Mater. Interfaces 10 (39) (2018) 33088–33096, https://doi.org/10.1021/acsami.8b13571.
[57] A. Tachibana, M.R. Santoso, M. Mahmoudi, P. Shukla, L. Wang, M. Bennett, A. B. Goldstone, M. Wang, M. Fukushi, A.D. Ebert, Y.J. Woo, E. Rulifson, P.C. Yang, Paracrine effects of the pluripotent stem cell-derived cardiac myocytes salvage the injured myocardium, Circ. Res. 121 (6) (2017) e22–e36, https://doi.org/10.1161/CIRCRESAHA.117.310803.
[58] K. Okita, Y. Matsumura, Y. Sato, A. Okada, A. Morizane, S. Okamoto, H. Hong, M. Nakagawa, K. Tanabe, K. Tezuka, T. Shibata, T. Kunisada, M. Takahashi, J. Takahashi, H. Saji, S. Yamanaka, A more efficient method to generate integration-free human iPS cells, Nat. Methods 8 (5) (2011) 409–412, https://doi.org/10.1038/nmeth.1591.
[59] R. Guo, F. Wan, M. Morimatsu, Q. Xu, T. Feng, H. Yang, Y. Gong, S. Ma, Y. Chang, S. Zhang, Y. Jiang, H. Wang, D. Chang, H. Zhang, Y. Ling, F. Lan, Cell sheet formation enhances the therapeutic effects of human umbilical cord mesenchymal stem cells on myocardial infarction as a bioactive material, Bioact. Mater. 6 (9) (2021) 2999–3012, https://doi.org/10.1016/j.bioactmat.2021.01.036.
[60] G.M. Fomovsky, S. Thomopoulos, J.W. Holmes, Contribution of extracellular matrix to the mechanical properties of the heart, J. Mol. Cell. Cardiol. 48 (3) (2010) 490–496, https://doi.org/10.1016/j.yjmcc.2009.08.003.
[61] N.G. Frangogiannis, The extracellular matrix in ischemic and nonischemic heart failure, Circ. Res. 125 (1) (2019) 117–146, https://doi.org/10.1161/CIRCRESAHA.119.311148.
[62] J. Bargehr, L.P. Ong, M. Colzani, H. Davaapil, P. Hofsteen, S. Bhandari, L. Gambardella, N. Le Novere, D. Iyer, F. Sampaziotis, F. Weinberger, A. Bertero, A. Leonard, W.G. Bernard, A. Martinson, N. Figg, M. Regnier, M.R. Bennett, C. E. Murry, S. Sinha, Epicardial cells derived from human embryonic stem cells augment cardiomyocyte-driven heart regeneration, Nat. Biotechnol. 37 (8) (2019) 895–906, https://doi.org/10.1038/s41587-019-0197-9.
[63] S.J. Park, R.Y. Kim, B.W. Park, S. Lee, S.W. Choi, J.H. Park, J.J. Choi, S.W. Kim, J. Jang, D.W. Cho, H.M. Chung, S.H. Moon, K. Ban, H.J. Park, Dual stem cell therapy synergistically improves cardiac function and vascular regeneration following myocardial infarction, Nat. Commun. 10 (1) (2019) 3123, https://doi.org/10.1038/s41467-019-11091-2.
[64] A.R. Williams, K.E. Hatzistergos, B. Addicott, F. McCall, D. Carvalho, V. Suncion, A. R. Morales, J. Da Silva, M.A. Sussman, A.W. Heldman, J.M. Hare, Enhanced effect of combining human cardiac stem cells and bone marrow mesenchymal stem cells to reduce infarct size and to restore cardiac function after myocardial infarction, Circulation 127 (2) (2013) 213–223, https://doi.org/10.1161/CIRCULATIONAHA.112.131110.
[65] E.M. Winter, A.A. van Oorschot, B. Hogers, L.M. van der Graaf, P.A. Doevendans, R.E. Poelmann, D.E. Atsma, A.C. Gittenberger-de Groot, M.J. Goumans, A new direction for cardiac regeneration therapy: application of synergistically acting epicardium-derived cells and cardiomyocyte progenitor cells, Circ Heart Fail 2 (6) (2009) 643–653, https://doi.org/10.1161/CIRCHEARTFAILURE.108.843722.
[66] J. Wang, S. Gu, F. Liu, Z. Chen, H. Xu, Z. Liu, W. Cheng, L. Wu, T. Xu, Z. Chen, D. Chen, X. Chen, F. Zeng, Z. Zhao, M. Zhang, N. Cao, Reprogramming of fibroblasts into expandable cardiovascular progenitor cells via small molecules in xeno-free conditions, Nat Biomed Eng 6 (4) (2022) 403–420, https://doi.org/10.1038/s41551-022-00865-7.

[67] P. Menasche, Cardiac cell therapy: current status, challenges and perspectives, Arch Cardiovasc Dis 113 (4) (2020) 285–292, https://doi.org/10.1016/j.acvd.2020.01.002.

[68] S. Sharma, R. Mishra, G.E. Bigham, B. Wehman, M.M. Khan, H. Xu, P. Saha, Y. A. Goo, S.R. Datla, L. Chen, M.E. Tulapurkar, B.S. Taylor, P. Yang, S. Karathanasis, D.R. Goodlett, S. Kaushal, A deep proteome analysis identifies the complete secretome as the functional unit of human cardiac progenitor cells, Circ. Res. 120 (5) (2017) 816–834, https://doi.org/10.1161/CIRCRESAHA.116.309782.

[69] T. Studemann, J. Rossinger, C. Manthey, B. Geertz, R. Srikantharajah, C. von Bibra, A. Shibamiya, M. Kohne, A. Wiehler, J.S. Wiegert, T. Eschenhagen, F. Weinberger, Contractile force of transplanted cardiomyocytes actively supports heart function after injury, Circulation 146 (15) (2022) 1159–1169, https://doi.org/10.1161/CIRCULATIONAHA.122.060124.

[70] M.J. Sebastiao, P. Gomes-Alves, I. Reis, B. Sanchez, I. Palacios, M. Serra, P. M. Alves, Bioreactor-based 3D human myocardial ischemia/reperfusion in vitro model: a novel tool to unveil key paracrine factors upon acute myocardial infarction, Transl. Res. 215 (2020) 57–74, https://doi.org/10.1016/j.trsl.2019.09.001.

[71] Z. Lin, P. Zhou, A. von Gise, F. Gu, Q. Ma, J. Chen, H. Guo, P.R. van Gorp, D. Z. Wang, W.T. Pu, Pi3kcb links Hippo-YAP and PI3K-AKT signaling pathways to promote cardiomyocyte proliferation and survival, Circ. Res. 116 (1) (2015) 35–45, https://doi.org/10.1161/CIRCRESAHA.115.304457.

[72] D.W. Sorensen, J.H. van Berlo, The role of TGF-beta signaling in cardiomyocyte proliferation, Curr. Heart Fail. Rep. 17 (5) (2020) 225–233, https://doi.org/10.1007/s11897-020-00470-2.

[73] G. Demetz, R.A.J. Oostendorp, A.M. Boxberg, W. Sitz, E. Farrell, B. Steppich, A. L. Steinsiek, M. Rudelius, I. Ott, Overexpression of insulin-like growth factor-2 in expanded endothelial progenitor cells improves left ventricular function in experimental myocardial infarction, J. Vasc. Res. 54 (6) (2017) 321–328, https://doi.org/10.1159/000479872.

[74] H. Li, F. Wu, G. Huang, D. Wu, T. Wang, X. Wang, K. Wang, Y. Feng, A. Xu, Cardiomyocytes induced from hiPSCs by well-defined compounds have therapeutic potential in heart failure by secreting PDGF-BB, Signal Transduct. Targeted Ther. 7 (1) (2022) 253, https://doi.org/10.1038/s41392-022-01045-4.

[75] S. Schafer, S. Viswanathan, A.A. Widjaja, W.W. Lim, A. Moreno-Moral, D. M. DeLaughter, B. Ng, G. Patone, K. Chow, E. Khin, J. Tan, S.P. Chothani, L. Ye, O. J.L. Rackham, N.S.J. Ko, N.E. Sahib, C.J. Pua, N.T.G. Zhen, C. Xie, M. Wang, H. Maatz, S. Lim, K. Saar, S. Blachut, E. Petretto, S. Schmidt, T. Putoczki, N. Guimaraes-Camboa, H. Wakimoto, S. van Heesch, K. Sigmundsson, S.L. Lim, J. L. Soon, V.T.T. Chao, Y.L. Chua, T.E. Tan, S.M. Evans, Y.J. Loh, M.H. Jamal, K. K. Ong, K.C. Chua, B.H. Ong, M.J. Chakaramakkil, J.G. Seidman, C.E. Seidman, N. Hubner, K.Y.K. Sin, S.A. Cook, IL-11 is a crucial determinant of cardiovascular fibrosis, Nature 552 (7683) (2017) 110–115, https://doi.org/10.1038/nature24676.

[76] O. Dewald, P. Zymek, K. Winkelmann, A. Koerting, G. Ren, T. Abou-Khamis, L. H. Michael, B.J. Rollins, M.L. Entman, N.G. Frangogiannis, CCL2/Monocyte Chemoattractant Protein-1 regulates inflammatory responses critical to healing myocardial infarcts, Circ. Res. 96 (8) (2005) 881–889, https://doi.org/10.1161/01.RES.0000163017.13772.3a.

[77] V. Kandalam, R. Basu, T. Abraham, X.H. Wang, P.D. Soloway, D.M. Jaworski, G. Y. Oudit, Z. Kassiri, TIMP2 deficiency accelerates adverse post-myocardial infarction remodeling because of enhanced MT1-MMP activity despite lack of MMP2 activation, Circ. Res. 106 (4) (2010), https://doi.org/10.1161/Circresaha.109.209189, 796-U334.

[78] Y. Tamura, H. Kohno, T. Mohri, Y. Fujio, G. Matsumiya, The cardioprotective effect of interleukin-11 against ischemia-reperfusion injury in a heart donor model, Ann Cardiothorac Sur 7 (1) (2018) 99–105, https://doi.org/10.21037/acs.2017.09.11.

[79] J. Ni, X. Liu, Y. Yin, P. Zhang, Y.W. Xu, Z. Liu, Exosomes derived from TIMP2-modified human umbilical cord mesenchymal stem cells enhance the repair effect in rat model with myocardial infarction possibly by the Akt/Sfrp2 pathway, Oxid. Med. Cell. Longev. (2019), 1958941, https://doi.org/10.1155/2019/1958941, 2019.

[80] S. Kurotsu, R. Osakabe, M. Isomi, F. Tamura, T. Sadahiro, N. Muraoka, H. Kojima, S. Haginiwa, H. Tani, K. Nara, Y. Kubota, M. Ema, K. Fukuda, T. Suzuki, M. Ieda, Distinct expression patterns of Flk1 and Flt1 in the coronary vascular system during development and after myocardial infarction, Biochem. Biophys. Res. Commun. 495 (1) (2018) 884–891, https://doi.org/10.1016/j.bbrc.2017.11.094.